Acid Base Properties of Coals and Coal Liquids

by

Edward M. Arnett* and Tanweer Ahsan

Department of Chemistry
Duke University
Durham, North Carolina 27706

Solution calorimetry provides a straightforward method for comparing the acid-base properties of solids with homogeneous analogues. The presentation will describe the correlations (and lack of them) between heats of interactions of a series of acids and a corresponding series of bases with several such heterogeneous/homogeneous systems. For example, solutions of p-toluenesulfonic acid are compared with slurries of sulfonic acid resins in their reactions with a series of nitrogen bases. Pyridine solutions are compared with slurries of polyvinylpyridine by their reactions with a series of carboxylic and sulfonic acids. Finally, several carefully chosen coal liquids are compared with related coals of different rank and are considered in the light of the above simpler systems.

Introduction

The classification of chemicals into acids and bases is one of the broadest in Science. It is well known that coals and the liquids derived from them include a number of functionalities and structures which are acidic (e.g., phenols, carboxylic acids) or basic (e.g., a variety of amino functions, ethers, sulfides and inorganic oxides). All types of organic functionalities are potentially basic towards protons, Lewis acids and hydrogen bond donors, and most of them are also acidic, in the Brönsted sense, if they carry protons bonded to carbon or other elements. However, only a few acidic or basic functionalities are strong enough to allow study in the familiar aqueous acid-base range of the pH meter. Over the past fifty years a variety of strategies have been developed for studying even very weak bases by reaction with strong superacids, and correspondingly weak acids with superbases. Of particular importance has been the development of gas phase techniques in the past fifteen years for studying proton transfer reactions in the gas phase which provides a very broad inherent scale of acid-base strengths from which all contributions due to solvation or ion-pairing effects have been completely removed.[1-5] The impact of gas phase studies on clarifying solvent effects can hardly be exaggerated.

The acid-base properties of solids play a fundamental role across a wide panorama of materials science, including among other matters corrosion, adhesion, the behavior of solid sensors, many biochemical medical and geochemical phenomena. Of great importance to the fossil fuel industry is the use of solid acid catalysts for a wide range of processes in the petroleum and coal derivative industries.

Unhappily, the methods for establishing quantitative acid-base scales for solids stand on a much sandier foundation than those used to compare liquid acid-base systems. A solid surface may carry a variety of basic sites in the presence of Lewis acid, Brönsted acid and hydrogen-bonding donor sites of widely different strengths and accessabilities. In solution a rapid equilibration is established between different types of acid or basic sites and it is reasonable to de-

scribe a solution as representing a single acidity or basicity value within a very limited range. One would scarcely think that after mixing a solution of hydrochloric acid with sodium hydroxide that there would coexist in solution a number of strongly acid and strongly basic sites. However, due to the inflexible structure of solids a material such as a Zeolite, alumina or coal may carry on its surface both acidic and basic sites that are permanently separated and do not interact with each other directly.

The Thermochemical Approach: A number of years ago we established a very simple thermochemical method for determining the strengths of basic liquids by measuring their heats of neutralization by a common very strong acid such as sulfuric or fluorosulfuric acid.[6] Samples of the base were injected directly with a Hamilton syringe into a calorimeter vessel full of the pure strong acid. Alternatively, the base could be titrated using a motor-drived burette into a vessel containing a solution of the acid in some relatively inert solvent such as acetonitrile. Heats of ionization were determined in this manner for a 100 or so bases of widely different type and were shown to correlate very well with the best results obtained by other much more laborious methods. Heats of ionization are a direct measure of basicity.

The great advantage of the calorimetric method is that it can also be applied with facility to the study of solid acids and bases using a stirred slurry of the solid under an inert solvent instead of the homogeneous solution of the acid or base. The thermochemical titration method, therefore, provides a direct means for comparing the acidity or basicity of homogeneous solutions with solids which are presumed to carry the same acid or base structure. This article provides a current overview of our use of the thermochemical method to compare several types of solid acids and bases with their homogeneous cognates. As a simple prototype example of a Brönsted acid Dowex polysulfonic acid resin was compared with p-toluenesulfonic acid solutions. A sample of Fisher silica was examined for its hydrogen-bonding acidity compared to p-fluorophenol. Polyvinylpyridine was compared to solutions of pyridine as a standard base, and Carbopack graphitized carbon was used as a model for the dispersion force interactions which inevitably contribute to adsorption of any gas or liquid on any type of solid. Finally, several types of well-characterized coals were compared with coal liquids derived from them.

Experimental

Surface areas were obtained by nitrogen adsorption at 77K employing the BET method and using a Quantachrome Surface area analyser. The acids and bases were obtained commercially and were used as 0.25-0.5 molar solutions in carefully purified acetonitrile or neat wherever indicated. Coal samples were obtained from Argonne Coal Bank, Exxon Research and Engineering Co. and Southern Electric International, Southern Clean Fuels Division at Wilsonville, Alabama.

Titration calorimetry using the Tronac 450 calorimeter is the most desirable technique for comparing heats of interaction of strong acids or bases with solids provided that the exothermic heats of interaction are large enough and are released in a relatively short period of time (say less than two minutes). In these cases the results can be expressed in terms of kcal/mol since it is known exactly how many moles of acid are required to titrate the solid. For titration calorimetry, the apparatus is calibrated every few weeks by measuring the heat of neutralization of aqueous sodium hydroxide by titration with standard aqueous hydrochloric acid $\Delta H = -13.42 \pm 0.39$ kcal/mol.

For cases where relatively small heats of interaction must be compared, and the total heat is given out over a long period (say one hour), heats of immersion are measured with the Seteram C-80 heat flow calorimeter. This instrument measures heats of immersion by releasing the solid base into a solution of the liquid acid or a neat liquid acid. Heats of immersion may also be obtained by sealing the solid in an ampule which is equilibrated thermally with the acid

solution and then crushed in the stirred calorimeter. For immersion calorimetry in contrast to titration calorimetry it is more realistic to present results in cal g^{-1} of solid base since there is no direct means of knowing how many moles of acid or base were actually involved in the interaction. We have used heats of dissolution of KCl in water as the calibrating standard for immersion calorimetry.

Heats of adsorption on Carbopack F were determined by gas-solid chromatography by the van't Hoff method previously described in which the retention volume of the adsorbate is studied as a function of temperature.

Results and Discussion

A prototype Brönsted solid acid Dowex---polysulfonic acid resin:[7] In order to establish the feasibility of the thermochemical method for comparing solid and homogeneous acids and bases, Dowex polysulfonic acid resin was treated as a slurry in acetonitrile with a series of nitrogen bases whose strength cover a reasonably wide range. The same bases were again injected into solutions of p-toluenesulfonic acid in acetonitrile and the heats of reaction determined. Although in aqueous solution neutralization would have occurred to produce dissociated ammonium and p-toluenesulfonate ions in acetonitrile, there is every reason to expect that hydrogen-bonded ion-pairs were produced according to equation 1.

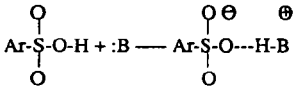

(1)

Figure 1 presents the excellent correlation between the two sets of enthalpy determinations. The quality of this correlation is of fundamental importance for our whole strategy for studying the strengths of solid acids and bases. Considering the above discussion of the real differences between the distribution of acid sites on various types of solid acids, the difference between chemisorption and physisorption, it would be possible that the difference between solid and liquid acid or base systems is inherently so great that no close correspondence between them could be found. Figure 1 emphasizes the fact that if there is ready access to surface acid sites of equivalent acidity that they respond proportionately in the same way as those same sites do if they are free molecular units in solution.

An instructive point in Figure 1 is its non-zero intercept indicating that the heats of interaction of the bases with PTSA are consistently 4-5 kcal/mol more exothermic than their interactions with Dowex resin. We have interpreted this in terms of the well-established stabilization of sulfonate anions in the presence of excess sulfonic acid according to Equation 2 which would be considerably easier in the solution phase reaction than on the solid surface where ionized sulfonate groups are separated in space from nearby unionized sulfonic acid groups. The difference of 4-5 kcal/mol is in exactly the appropriate range for the formation of such a hydrogen-bond stabilized anion.

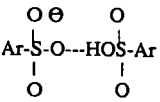

(2)

Polyvinylpyridine a prototype solid base: Following the strategy described above, a thermochemical comparison has been made between solutions of pyridine and polyvinylpyridine

in which pyridine units are attached to an extended carbon framework. Figure 2 provides exactly the same type of correlation for these liquid and solid basic systems as those presented in Figure 1 for liquid and solid acids. We believe that it is significant that in this case the intercept is within experimental error of zero which helps to support the explanation given above for the non-zero intercept in the case of the sulfonic acids. In the case of protonating the pyridines the sulfonate and carboxylate anions are left free in solution where they can be stabilized in exactly the same way (Equation 2) after reaction with free pyridine molecules or pyridine units attached to the polymeric framework.

Silica a hydrogen-bonding acid: Silica is probably one of the best characterized and best understood of solid acids.[9] Its interaction with bases, unless they are unusually strong, is usually through hydrogen-bonding from the hydroxyl groups on the silica surface. In order to probe the use of silica as a prototype hydrogen-bonding acid, a standard sample of Fisher silica was treated with a series of nitrogen and oxygen bases which are well-established as hydrogen-bond acceptors.[10] Figure 3 shows the relationship between these heats of interaction and the corresponding heats of interaction for the same series of bases with p-fluorophenol, a well-established hydrogen-bonding acid. Although the correlations are not as good as those shown in Figures 1 and 2, it is apparent that the heats of interaction of the bases with silica is indeed largely determined by hydrogen-bonding.

Since hydroxyl groups are amphiprotic, amphoteric functionalities, we tried examining silica as an acceptor base for hydrogen bonds or protons from the same series of acids used with pyridine and polyvinylpyridine.[11] To our surprise, the heats of interaction followed an entirely different pattern than would have been expected if the acids were donating protons or hydrogen bonds to silica. Instead, the simplest interpretation of the results was that the silica was actually serving as a strong hydrogen-bonding acid that it was donating hydrogen bonds to the carboxcylic and sulfonic acid functionalities instead of receiving protons from them.

Physisorption on Carbopack carbon: All matter attracts all matter through dispersion force interactions and accordingly, in the absence of all other types of interactions, gases and liquids will be adsorbed on any kind of solid. As a prototype dispersion force adsorbent we chose Carbopack F, a graphitized carbon, and determined the heats of adsorption of a variety of compounds on the surface using the van't Hoff equation and the temperature dependence of gas chromatographic retention volumes as the experimental tool.[12] It was immediately apparent from the results when compared with those presented in Figures 1 and 2 that the heats of adsorption had absolutely no relation whatsoever to the basicities or acidities of the adsorbed molecules. Instead, excellent correlations were found (Figures 4 and 5) between the simple number of main group atoms in the adsorbates and their total polarizabilities (the dipole polarizability plus the electronic polarizability).

Comparison of solid coals and coal liquids: The rest of this paper will present work mainly acquired during the summer from the heats of reaction of several well-classified coal liquids received from the Southeast Regional Laboratory at Wilsonville, Alabama and titration of slurries with the corresponding coals from which the coal liquids were derived.

References

1. Aue, D.H.; Bowers, M.T. *In Gas Phase Ion Chemistry*; Bowers, M.T.; Ed.; Academic Press: New York, 1979; Vol 2, pp 1-51 and references therein.

2. Lias, S.G.; Liebman, J.F.; Levin, R.D. *J. Phys. Chem.* Ref. data, **1984**, 13, 3, 695-808.

3. Taft, R.W. in *Progress in Physical Organic Chemistry*, John Wiley & Sons: New York, 1983, Vol 14, pp 247-350.

4. Arnett, E.M. Acc. Chem. Res. **1973**, *6*, 404.

5. Epshtein, L.M. Russ. Chem. Rev. **1979**, *48(9)*, 854.

6. a) Arnett, E.M.; Burke, J.J. *J. Am. Chem. Soc.* **1966**, *88*, 4308.
   b) Arnett, E.M.; Quirk, R.P.; Burke, J.J. *J. Am. Chem. Soc.* **1970**, *92*, 1260.
   c) Arnett, E.M.; Quirk, R.P.; Larsen, J.W. *J. Am. Chem. Soc.* **1970**, *92*, 3977.
   d) Arnett, E.M.; Mitchell, E.J.; Murty, T.S.S.R. *J. Am. Chem. Soc.* **1974**, *96*, 3875.

7. Arnett, E.M.; Haaksma, R.A.; Chawla, B.; Healy, M.H. *J. Am. Chem. Soc.* **1986**, *108*, 4888.

8. Arnett, E.M. Ahsan, T.; Amarnath, K. in press.

9. a) Iler, K.R. *The Chemistry of Silica*, John Wiley and Sons, 1979.
   b) Legrand, A.P.; et al., *Adv. in Coll. & Interf. Sci.* **1990**, *33*, pp 91-330.
   c) Morrow, B.A.; McFarlan, A.J. *J. Non-Cryst. Solids* **1990**, *120*, 61.
   d) Nawrocki, J. *Chromatographia* **1991**, *31(3-4)*, 177.
   e) Nawrocki, J. *Chromatographia* **1991**, *31(3-4)*, 193.

10. Arnett, E.M.; Cassidy, K.F. *Rev. Chem. Intermed.* **1988**, *9*, 27.

11. Arnett, E.M.; Ahsan, T. in press.

12. Arnett, E.M.; Hutchinson, B.J.; Healy, M.H. *J. Am. Chem. Soc.* **1988**, *110*, 5255.

Figure 1

Plot of ΔH_{Dowex} Vs. ΔH_{PTSA} with various bases at 25° C

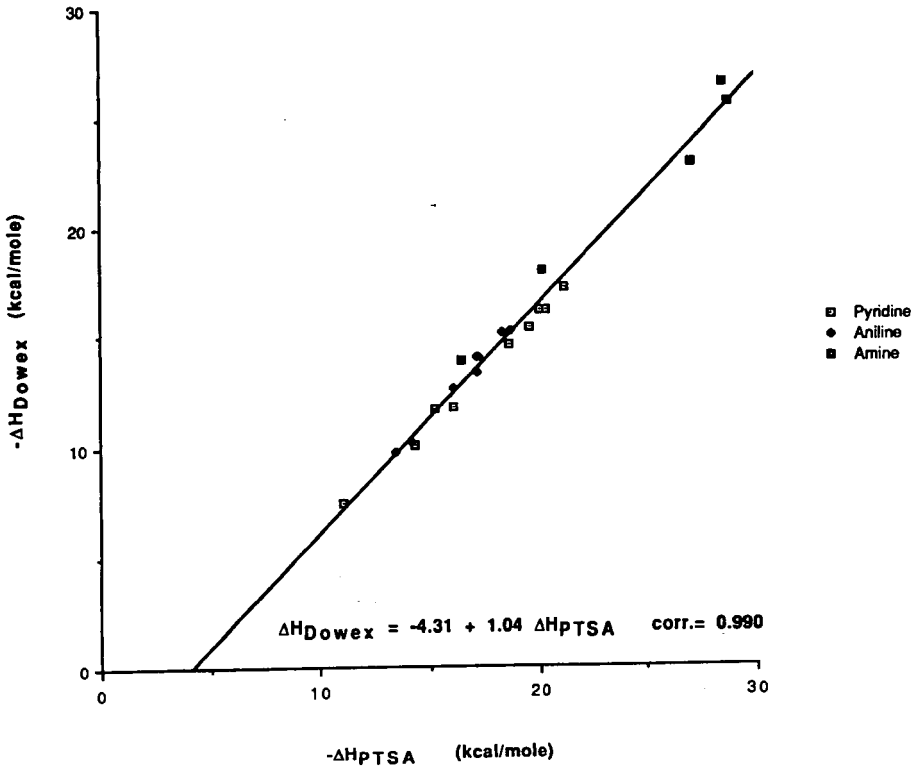

Figure 2

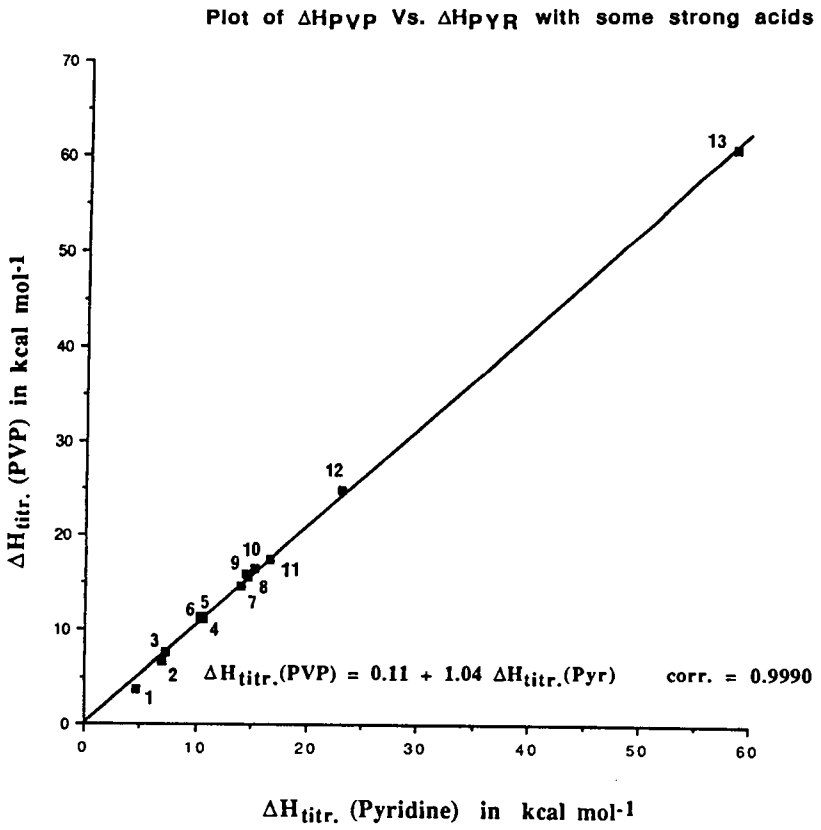
Plot of ΔHpVP Vs. ΔHpYR with some strong acids
ΔHtitr. (PVP) in kcal mol-1
ΔHtitr. (Pyridine) in kcal mol-1
ΔHtitr.(PVP) = 0.11 + 1.04 ΔHtitr.(Pyr)
corr. = 0.9990
0
10
20
30
40
50
60
70
1
2
3
4
5
6
7
8
9
10
11
12
13

Figure 3

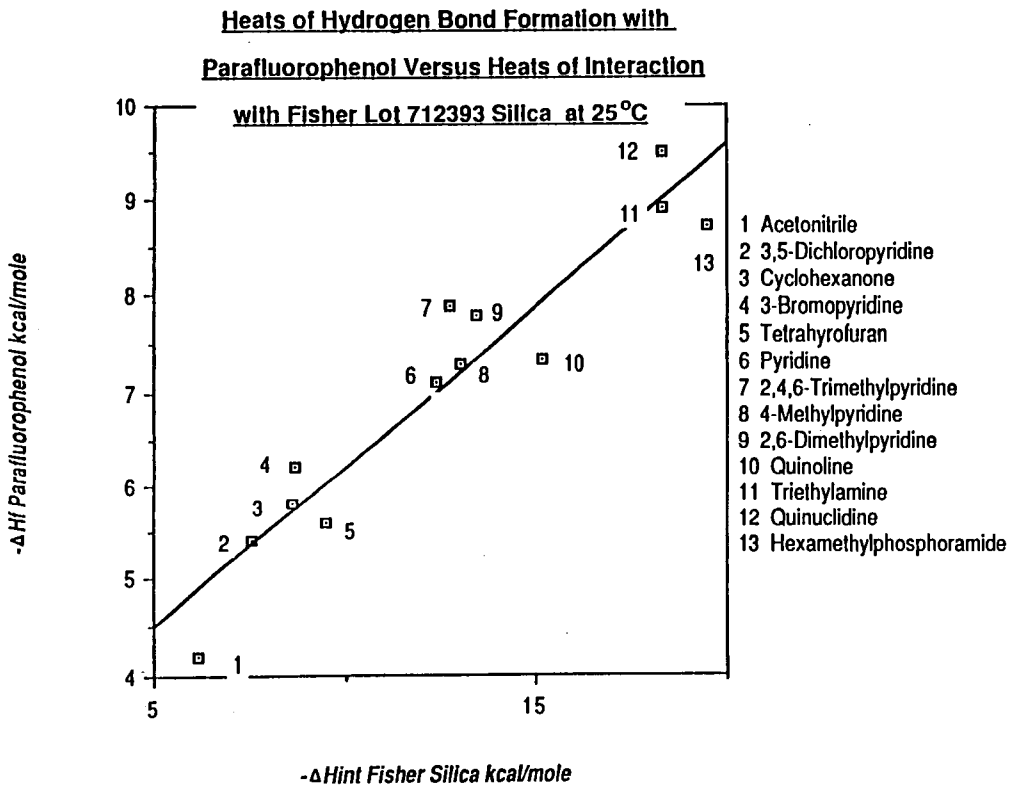
Heats of Hydrogen Bond Formation with
Parafluorophenol Versus Heats of Interaction
with Fisher Lot 712393 Silica at 25°C
-ΔHf Parafluorophenol kcal/mole
-ΔHint Fisher Silica kcal/mole
10
9
8
7
6
5
4
5
15
1 Acetonitrile
2 3,5-Dichloropyridine
3 Cyclohexanone
4 3-Bromopyridine
5 Tetrahyrofuran
6 Pyridine
7 2,4,6-Trimethylpyridine
8 4-Methylpyridine
9 2,6-Dimethylpyridine
10 Quinoline
11 Triethylamine
12 Quinuclidine
13 Hexamethylphosphoramide

Figure 4

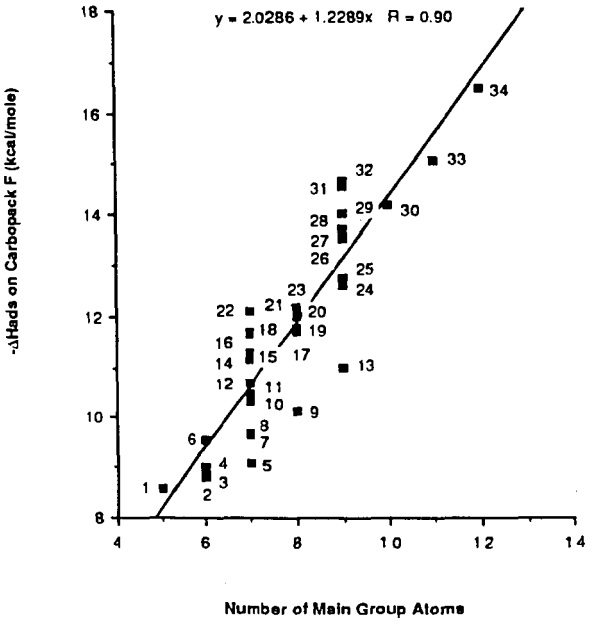

1. *n*-Butylamine
2. *n*-Pentanol
3. Pyridine
4. Benzene
5. Cyclohexanol
6. Hexane
7. Cyclohexanone
8. Cyclohexylamine
9. Methyl valerate
10. *n*-Hexanol
11. Toluene
12. 2-Methylpyridine
13. Methyl caproate
14. 3-Methylpyridine
15. 4-Methylpyridine
16. *n*-Hexylamine
17. *m*-Cresol
18. Bromobenzene
19. Benzonitrile
20. Octane
21. 2,6-Lutidine
22. 1-Bromohexane
23. Anisole
24. *n*-Octanol
25. Nitrobenzene
26. 2,4,6-Collidine
27. Nonane
28. Octylamine
29. 1-Chlorooctane
30. *n*-Butylbenzene
31. *o*-Bromoanisole
32. *p*-Bromoanisole
33. Undecane
34. Dodecane

Heats of Adsorption of a Variety of Adsorbates on Carbopack F *versus* the Number of Main Group Atoms.

Figure 5

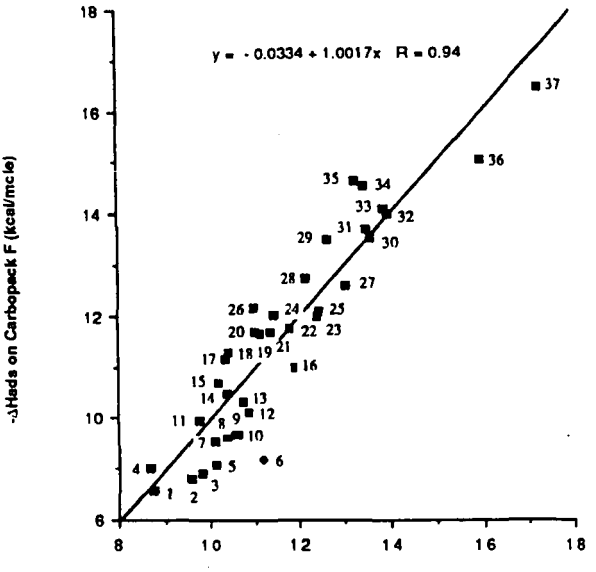

-ΔHcalc = 0.646(electronic polarizability) + 0.015 (orientation polarizability) + 2.410

1. *n*-Butylamine
2. *n*-Pentanol
3. Pyridine
4. Benzene
5. Cyclohexanol
6. Triethylamine
7. Hexane
8. Cyclohexanone
9. Dimethyl sulfoxide
10. Cyclohexylamine
11. Propylene carbonate
12. Methyl valerate
13. *n*-Hexanol
14. Toluene
15. 2-Methylpyridine
16. Methyl caproate
17. 3-Methylpyridine
18. 4-Methylpyridine
19. *n*-Hexylamine
20. *m*-Cresol
21. Bromobenzene
22. Benzonitrile
23. Octane
24. 2,6-Lutidine
25. 1-Bromohexane
26. Anisole
27. *n*-Octanol
28. Nitrobenzene
29. 2,4,6-Collidine
30. Nonane
31. Octylamine
32. 1-Chlorooctane
33. *n*-Butylbenzene
34. *o*-Bromoanisole
35. *p*-Bromoanisole
36. Undecane
37. Dodecane

Heats of Adsorption on Carbopack F *versus* Electronic plus Orientation Polarizability.

SHORT RANGE RING STRUCTURING IN A META-ANTHRACITE COAL

David L. Wertz
Department of Chemistry & Biochemistry
University of Southern Mississippi
Hattiesburg, MS 39406-5043

Key Phrases: Molecular scattering, graphitic layers, cluster size

INTRODUCTION

X-ray characterizations of coals and coal products have occurred for many years.[1-9] Hirsch and Cartz[1], several years ago, measured the diffraction from several coals over the reciprocal space region from X = 0.02 $Å^{-1}$ to 1.2 $Å^{-1}$ (X = [2/λ]·sinθ). In these studies, a 9 cm powder camera was used to study the high angle region, and a transmission type focussing camera equipped with a LiF monochromator was used for the low angle measurements. They reported that the height of the [002] peak (at ca. 3.5 Å) measured for each coal is proportional to the % carbon in several coals. Hirsch[2] also suggests that the Pontyberem anthracite (94.1% carbon, 3.0% hydrogen, and 5.3% volatile matter with a specific gravity of 1.46) has a layer diameter of ca. 16 Å corresponding to an aromatic lamellae of ca. C_{87}. For coals with lower carbon content, Hirsch proposes much smaller lamellae; C_{19} for a coal with 80% carbon, and C_{24} for a coal with 89% carbon.

Because of the importance placed by coal scientists on correctly characterizing the nature of the cluster(s) in coals and because of improvements in both x-ray experimentation capabilities and computing power, we have measured the x-ray diffraction and scattering produced from irradiation of a meta-anthracite coal[10] with hard xrays.[11] The objective of our study is to determine the intra-planar, and where possible inter-planar, structural details of coals and to determine the extent to which layering in coals mimics that of crystalline graphite and/or synthetic polymers. To accomplish the former we have utilized the methods normally used for the molecular analysis of non-crystalline condensed phases such as liquids, solutions, and amorphous solids.[12-23]

The coal, a meta-anthracite which was derived from the Portsmouth, RI mine (southeastern Narragansett Basin), was supplied to us by Professor James W. Skehan, S. J. of the Department of Geology and Geophysics at Boston College.

Reported herein are the results obtained from the hard x-ray analysis of this coal.

EXPERIMENTAL

META-ANTHRACITE COAL. From a 10 gram sample of the coal, a 3 gram aliquot was ground into a fine powder using our SPEX ball mill. The resulting powdered coal was passed through a -100 mesh filter.

A 0.4869 g sample of the finely ground powder was mounted onto a PVC sampleholder and mounted into the x-ray diffractometer.

X-RAY EXPERIMENTS. Mo xrays were used as the exciting radiation. The diffractometer was equipped with a θ-compensating slit, a sample spinner, and a LiF crystal in the secondary x-ray beam.[11] A diffraction pattern of the powdered coal mounted onto the PVC substrate was obtained by collecting intensities for five second intervals at $d2\theta = 0.01^\circ$ over the range from $2\theta = 8.00^\circ$ to $2\theta = 120.00^\circ$. The diffraction pattern from the PVC sampleholder was obtained using exactly the same protocol.

A diffraction pattern of a 0.3878 g sample of reagent grade graphite (Alfa Products) was obtained using the same sampleholder and methodology.

RESULTS AND DISCUSSION

Shown in Figure 1 is the diffractogram of the meta-anthracite sample as well as the diffractogram of the graphite sample.

THE 3.4 Å DIFFRACTION PEAK. The location of this large peak in the meta-anthracite diffractogram corresponds to the [002] diffraction peak which dominates the diffraction pattern of graphite (d = 3.37 Å). Hirsch[1,2] and Franklin[3] report this peak at 3.5 Å in previous studies. Ebert, Scanlon, and Clausen[12] find a similar large first peak in the diffractogram of a combustion tube soot. Comparison of the diffractograms indicates that while the first peaks occur at ca. 3.4 Å, the details of these peaks are quite dissimilar, suggesting that the regularity of the inter-planar spacings, reported to be the cause of 3.4 Å peak, is considerably less in this meta-anthracite than in graphite.

AMORPHOUS SCATTERING DUE TO THE CARBONACEOUS CONTENT OF THE META-ANTHRACITE. Shown in Figure 2 is the separation of the diffraction peaks (2A) from the molecular scattering (2B) for the meta-anthracite. The molecular scattering curve, $I_A(2\theta)$, is similar in shape to the scattering curve obtained previously for an amorphous carbon black,[6] and also to the scattering curves measured for liquids, solutions, and other amorphous solids.[12-23]

The molecular scattering was fitted to the independent scattering curve[24-26] to obtain the reciprocal space interference curve i(s) where $s = (4\pi/\lambda)\sin\theta$. The latter is a description of the average 1-dimensional structural features of the meta-anthracite.

Using conventional methods the atom-pair radial-distribution function was calculated for the meta-anthracite from its

interference function via Fourier transform. The APRDF (Figure 4) provides a measure of the atom-pair distances and their relative importance in the non-crystalline material. The APRDF contains major peaks centered at 1.40 Å, 2.42 Å, 2.85 Å, 3.6 Å, 4.8 Å, 6.0 Å and to r → 15 Å.

P_1 (centered at 1.40 Å) is due to the bonded C-C distance, i.e. C_r-C_1 in Figure 3. The 2.42 Å peak (P_2) is due to the nearest non-bonded C··C atom-pairs. From P_1 and P_2, the average C-C-C bond angle was calculated to be 120° (±4°). P_3 (centered at 2.84 Å) is also attributed to non-bonded C··C atom-pairs. The relative P_1, P_2, and P_3 distance and magnitudes as well as the C-C-C bond angle indicate that the average PAH ring is quite similar to those found in anthracene, napthalene, and pyrene.[27-32] The remaining several peaks in the RDF are due to inter-ring C··C atom-pairs and are being used to estimate the planarity and size of the average PAH cluster in the meta-anthracite. Our results will be compared to those presented by other investigators.[33-39]

REFERENCES

1. Cartz, L. and Hirsch, P. B., 1960 (252) 68.
2. Hirsch, P. B., 1954 (226) 143.
3. Franklin, R. E., Acta Crystallogr., 1950 (3) 10.
4. Kwan, J. T. and Chen, T. F., Proc. Div. Fuel Sci., 1976 (21) 67.
5. Diamond, R., Act Crystallogr., 1958 (11) 129.
6. Wertz, D. L., Powder Diff., 1988 (3) 153.
7. Wertz, D. L., Smithhart, C. B., and Wertz, S. L., Adv. X-Ray Anal., 1990 (33) 475.
8. Davis, B. L., Powder Diffr.,.1986 (1) 244.
9. McCarthy, G. J., Powder Diffr., 1986 (1) 50.
10. Skehan, J. W., Rast, N., and Mosher, S., "Paleonenvironmental and Tectonic Controls of Sedimentation in Coal-Forming Basins of Southeastern New England", Geological Society of America, Special Paper 210, 1986; Skehan, J. W. and Rast, N., Pre-Mesozoic Evolution of Avalon Terranes of Southern New England. Geological Society of America, Special Paper 245, 1990.
11. Wertz, D. L., Powder Diffr., 1990 (5) 44.
12. Mitchell, G. R. and Windle, A. H., J. Appl. Crystallogr., 1980 (13) 135.
13. Wertz, D. L. and Kruh, R. F., J. Chem. Phys., 1967 (47) 388.
14. Levy, H. A., Danford, M. D., and Narten, A. H., ORNL Report No. 3960, 1966.
15. Harris, R. W. and Clayton, G. T., J. Chem. Phys., 1966 (45) 2681.
16. Ohtaki, H. and Wada, H., J. Solution Chem., 1985 (14) 3.
17. Lovell, R., Mitchell, G. R., and Windle, A. H., Acta Crystallogr., 1979 (A35) 598.
18. Johansson, G. and Wakita, H., Inorg. Chem., 1985 (24) 3047.
19. Yamaguchi, T. S., Hayashi, T., and Ohtaki, H. Inorg. Chem., 1989 (28) 2434.
20. Bell, J. R., Tyvoll, J. L., and Wertz, J. Am. Chem. Soc., 1973 (95) 1456.
21. Wertz, D. L. and Hicks, G. T., J. Phys. Chem., 1980 (84) 521.
22. Wertz, D. L. and Holder, A. J., J. Phys. Chem., 1987 (91) 3479.
23. Wertz, D. L. and Cook, G. A., J. Solution Chem., 1985 (14) 41.
24. Hajdu, F., Acta Crystallogr., 1971 (A27) 73; 1972 (A28) 250; Palinkos, G., private communications, 1980.
25. Kruh, R. F., Chem. Rev., 1962 (62) 319.
26. Konnert, J. H. and Karle, J., Acta Crystallogr., 1973 (A29).
27. Cruickshank, D. W. J., Acta Crystallogr., 1959 (12) 208.
28. Abrahams, S. C., Robertson, J. M., and White, J. G., Acta Crystallogr., 1949 (2) 233.
29. Cruickshank, D. W. J., Acta Crystallogr., 1957 (10) 504.
30. Ahmed, F. R. and Cruickshank, D. W. J., Acta Crystallogr., 1952 (5) 852.
31. Cruickshank, D. W. J., 1956 (9) 915.
32. Robertson, J. M. and White, J. G., J. Chem. Soc., 1947 358.
33. Solum, M. S., Pugmire, R. J., and Grant, D. M., Energy Fuels, 1989 (3) 187.
34. Sethi, N. K., Pugmire, R. J., Facelli, J. C., and Grant, D. M., Anal. Chem., 1988 (60) 1574.
35. Murphey, P. D., Cassady, J. J., and Gerstein, B. C., Fuel, 1981 (61) 1233.
36. Miller, D. J., Hawthorne, S. B., and Timpe, R. C., Div. Fuel Chem. Am. Chem. Soc., 1988 (33) 455.
37. Wornat, M. J., Sarofim, A. F., and Longwell, J. P., Energy Fuels, 1987 (1) 431.
38. Aigbehinmua, H. B., Darwent, J. R., Gaines, A. F., Energy Fuels, 1987 (1) 386.
39. Wertz, D. L., Bissell, M., and Vorres, K. S., unpublished results, 1991.

FIGURE ONE. DIFFRACTOGRAMS

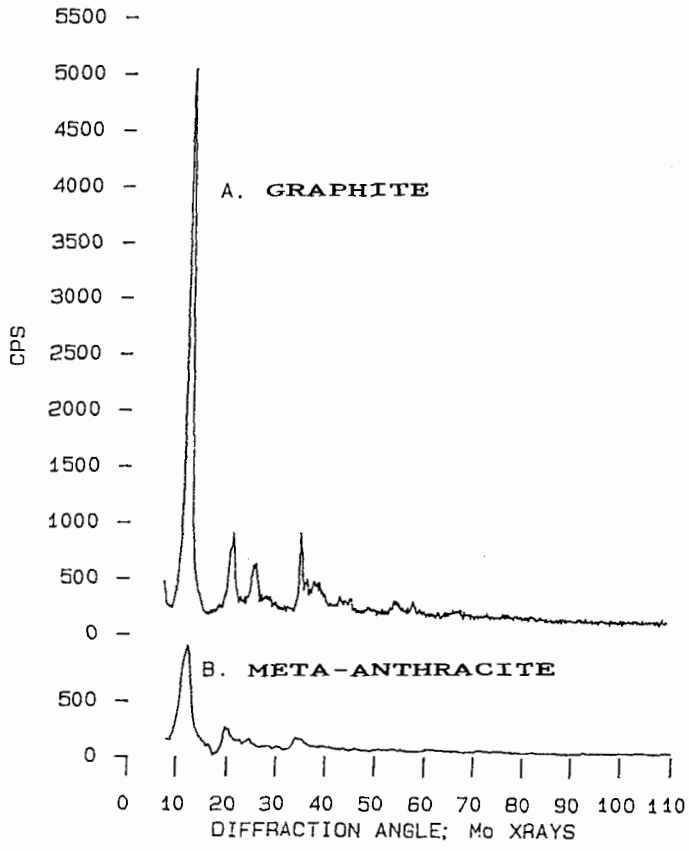

FIGURE TWO. SEPARATION OF DIFFRACTOGRAM INTO COMPONENTS

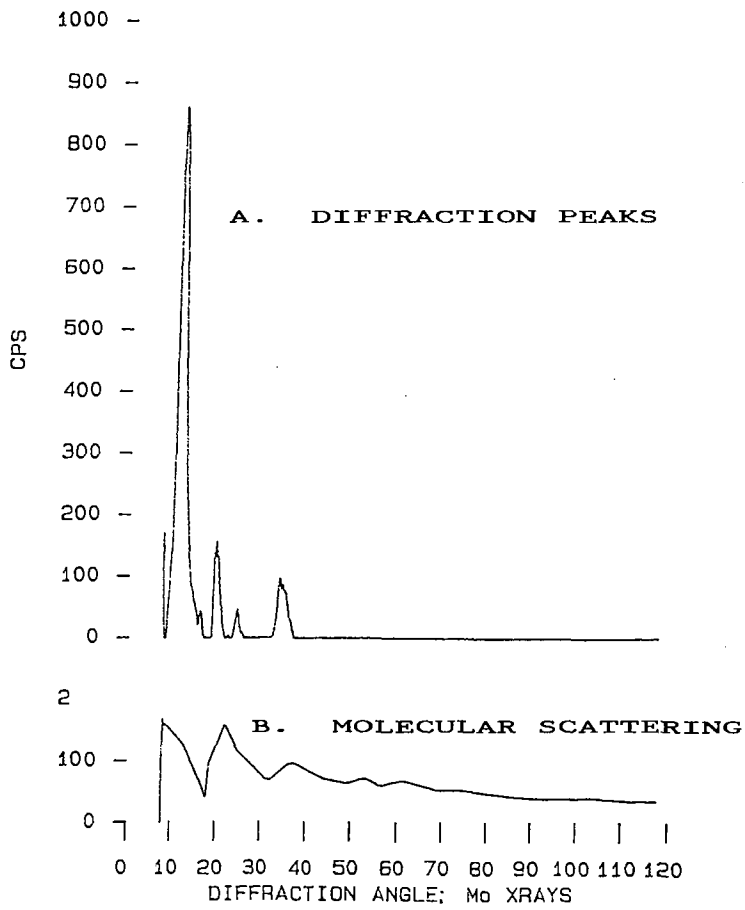

FIGURE THREE. RECIPROCAL SPACE FUNCTIONS

3A. Molecular Scattering Curve (dots)
3B. Calculated Independent Atom Scattering Curve
3C. Interference Curve

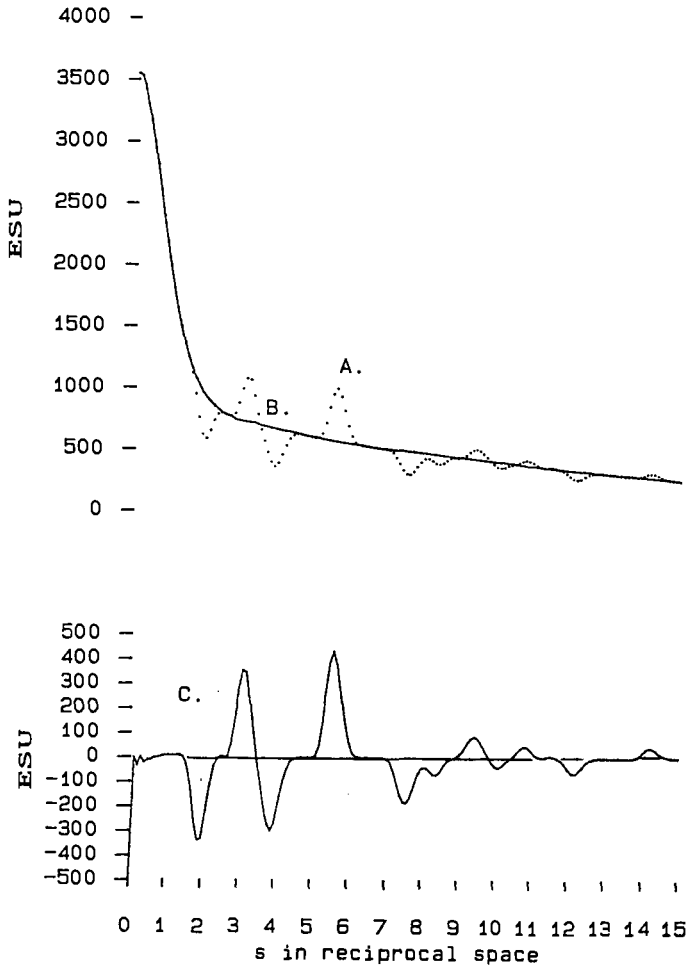

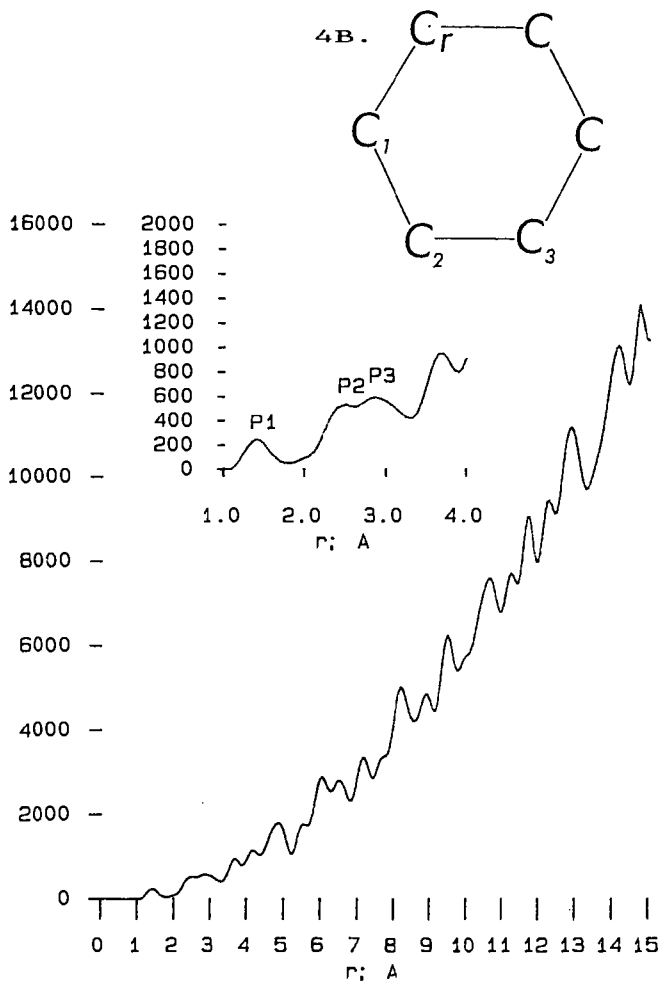

FIGURE FOUR. THE APRDF AND AN AROMATIC RING (4B)

Development of Computer-Controlled Scanning Electron Microscopy (CCSEM) Techniques for Determining Mineral-Maceral Association

G. P. Huffman, N. Shah, and F. E. Huggins, 233 Mining & Mineral Res. Bldg., University of Kentucky, Lexington, KY 40506-0107
and
G. S. Cassucio and W. J. Mershon, RJ Lee Group, Inc., 350 Hochberg Rd., Monroeville, PA 15146

I. INTRODUCTION

The solutions to several important problems in coal science depend critically on being able to determine mineral-maceral association. Perhaps the most obvious of these is physical coal cleaning. Liberated or nearly liberated mineral matter will normally be most easily removed in advanced physical cleaning processes, such as froth or microbubble flotation or oil agglomeration. Although the oxidation state of the coal and mineral particle surfaces also plays an important role,[1] it is generally felt that liberation is the primary factor in determining coal cleanability by physical methods.

A second topic that is receiving increasing attention is the effect of mineral-maceral association on ash slagging and fouling behavior during coal combustion.[2] Slagging behavior is usually more severe under reducing combustion conditions than under oxidizing conditions. This is primarily because ferrous iron derived from pyrite reacts more readily with clay minerals and quartz to form molten slag than does ferric iron.[3] Thus, quantitative determinations of the amounts and types of mineral matter and carbonaceous material associated together in coal particles may be useful in predicting slagging distributions on a particle by particle basis.

Recently, Straszheim, Markuszewski and coworkers[4] have succeeded in making the first quantitative measurements of the association of mineral matter with the organic coal matrix using CCSEM. By mounting the crushed coal in carnauba wax, which has an average atomic number that is somewhat lower than coal, they were able to clearly distinguish between the mounting medium and the coal in the backscatter electron imaging (BEI) mode. A CCSEM automatic image analysis (AIA) procedure was used to determine the amounts of different minerals and the amount of organic matter ("coal") associated with each particle on a particle by particle basis. This allowed them to determine the amounts of each major mineral (pyrite, kaolinite, illite, etc.) associated with various amounts of coal (0 - 20%, 20 -40%, etc.).

In the current research, we have investigated mineral-maceral (the term "maceral" is used here in the generic sense) association using a somewhat different approach. Specifically, we are attempting to combine the use of a digital imaging technique called "microimaging"[5,6] with ternary and quaternary representations[7,8] of particle chemistry determined from energy dispersive x-ray (EDX) spectra obtained using a light element detector. The results indicate that this approach is rather promising.

II. EXPERIMENTAL PROCEDURE

Ternary diagram representation of CCSEM EDX data has proven to be very useful in allowing graphic interpretation of trends that develop in particle chemistry as a result of various types of processing or reaction. Previously, we have used this method for investigating reactions that occur between different minerals during coal combustion[7,8] and carbonization[9]. Briefly,

three elements are selected and one or more thresholds are set as a basis for admitting a given particle into the data set. For example, in the current investigation, mineral-maceral association is of primary interest, so we have examined C - S - Fe diagrams, which are representative of pyrite - coal maceral association. The approximate chemical compositions of the particles are calculated from the raw EDX spectra using the background-subtracted peak areas. Several variations on this basic presentation proved to be very useful. For example, the sum of two or more elements can be used as a vertex and the diagram C - (Fe + S) - (Al + Si) is effectively a coal - pyrite - clay/quartz diagram. Additionally, the number or percentage of particles in a given compositional increment can be displayed in a four dimensional graph, which provides a much more vivid representation of the particle-by-particle compositional trends. Such frequency-composition dependence may also be presented in binary form across any linear strip of the ternary diagram. Finally, particle size histograms for any user-selected composition range are readily generated in a cursor-window mode.

The coals investigated in this study were Illinois #6 samples obtained from the Argonne Premium Coal Sample Bank (APCSB)[10] and from the University of Kentucky Center for Applied Energy Research (CAER).[11] The APCSB coal was hand ground to 100% -200 mesh (<75 microns) before investigation; a simple laboratory cleaning process was used for this sample, which consisted of floating the coal in carbon tetrachloride and centrifuging. The CAER sample was micronized to <10 - 20 microns and cleaned using a column flotation process discussed in detail elsewhere.[12]

One method of sample preparation used was essentially identical to that developed by Straszheim et al.;[4] that is, the coal powder was mixed with molten carnauba wax, pressed into a pellet in a hydrostatic press, and polished using petrographic methods with diamond paste (< 1 micron) finish. The second method consisted of dispersing the particles directly onto a beryllium (Be) substrate.

The basic CCSEM analysis is conducted in the usual manner,[13,14] by moving the electron beam over the sample in discrete increments, measuring the backscattering electron intensity (BEI) at each stopping point, and collecting an energy dispersive x-ray spectrum (EDX). In the current work, the discrimination level discerning particles from background was set low enough to allow coal maceral material to be detected, as opposed to the usual CCSEM mode for coal[13,14], in which only minerals are detected. The EDX spectra were then collected over a period of 15 seconds while the electron beam was rastered over the whole coal particle. Since a light element detector was used, the resulting EDX spectra were characteristic of whole coal particles, including both mineral and maceral material. An additional novel feature of the current work was the simultaneous acquisition and storage on disks of digital images of all particles, a procedure called microimaging,[5,6] which will be addressed in a future paper.

III. RESULTS AND DISCUSSION

The principal results are best summarized by perspectively plotted phase diagrams in which number percentage is shown as a fourth, vertical dimension. The C-S-Fe diagrams in figures 1 and 2 illustrate the degree of liberation of pyrite in the -200 mesh Illinois No. 6 coal and the extent of its removal in a simple laboratory cleaning operation, centrifugation in carbon tetrachloride. These diagrams have been drawn using a rather low threshold value of C + S + Fe > 15%; therefore most of the coal particles examined are represented in the diagrams. It is seen by comparison of Figures 1 and 2 that the two sample preparation methods gave results that are qualitatively similar. Presumably, the samples prepared by dispersal of the coal particles onto beryllium give EDX spectra that are more characteristic of the coal particle surfaces than the polished carnauba wax samples, since the electron beam penetrates only a few

microns into the coal and the particles in the polished specimens are cross-sectioned, on average. This suggests that the distribution of pyrite on the surfaces of the crushed coal particles is not markedly different from its bulk distribution for this particular coal.

It is evident that most particles containing < 30 - 40% C on the basis of the EDX spectra have been removed in the cleaning operation. It must be noted, however, that the compositions shown in these diagrams have not been corrected for preferential absorption of the low energy carbon X-rays (277 eV) relative to the absorption of the higher energy sulfur (2308 eV) and iron (6404 eV) X-rays, which occurs primarily in the thin window of the light element detector. Such corrections are important if we wish to use such diagrams as quantitative composition guides. For example, the particles having compositions along the C-S border represent coal particles that contain primarily organic sulfur. With appropriate calibration of the relative strengths of the C and S X-rays, such data could be used to make direct measurement of the organic sulfur content on a particle by particle basis.

An alternative way of presenting the data is shown in Figures 3 to 5. Here, the corners of the diagram are C, (Fe + S), and (Al + Si), and the threshold is taken as 80%. As seen from the number of particles plotted, this encompasses nearly the whole data set. With this representation, the vertexes for these diagrams are effectively coal (that is, mineral free coal particles), pyrite, and clay plus quartz (Figures 3 - 5). This representation has the advantage of illustrating the efficiency of a given cleaning process for removing all of the major minerals in coal, not just pyrite. It is seen from the perspectively plotted ternary diagrams (Figures 3 - 5) that the two methods of sample preparation give results that are significantly different for the clay/quartz abundance in the as-crushed coal. Presumably, this indicates that this coal fractures most easily along clay-coal interfaces. This would cause the sample prepared by dispersion of the coal particles onto beryllium to exhibit a higher percentage of clay/quartz rich particles than the polished carnauba wax-mounted specimen, since the EDX spectra are derived primarily from the top 1 - 2 microns of the coal. The results for the cleaned coals are again qualitatively similar for the two sample preparations, with most of both the pyrite and clay/quartz having been removed.

A sample of Illinois No. 6 coal was also examined before and after a column froth floatation cleaning process described in more detail elsewhere.[12] Only the sample preparation method of dispersing coal particles onto a beryllium disk was used for these samples. Results for the feed coal, which is micronized to < 10 to 20 microns, are shown in the top half of Figure 11. It is seen that these coal particles exhibit a heavy preponderance of clay minerals, again indicating a tendency of the coal to fracture at coal-clay interfaces. In the column floatation process, both the ash and pyritic sulfur are dramatically reduced, as shown by the perspective ternary diagram in the bottom half of Figure 5.

Such CCSEM diagrams could be very useful in predicting cleaning behavior of individual mineral species. One can easily envision cases where it is easier to remove pyrite than clays and quartz and vice-versa. Certain types of cleaning operations could then substantially change the slagging and fouling behavior of a coal.

IV. SUMMARY AND CONCLUSIONS

In this research, the feasibility of determining mineral-maceral ("maceral" is used in the generic sense) association using four-dimensional ternary composition - number percentage diagrams generated from CCSEM data has been investigated. The results indicate that this approach is promising. The degree of liberation of pyrite and its removal during physical cleaning is perhaps most clearly illustrated by perspectively plotted C - S - Fe diagrams with number percentage shown as a fourth vertical ordinate (Figures 1 and 2). Alternatively, a C -

(Fe + S) - (Al + Si) ternary diagram is effectively a coal - pyrite - clay/quartz ternary. Four dimensional frequency of occurrence - coal - pyrite - clay/quartz diagrams (Figures 3 - 5) illustrate the degree of liberation and removal during cleaning of most of the principal minerals in coal. They also indicate a marked tendency of Illinois #6 coal to fracture at coal - clay interfaces.

Future papers will discuss other aspects of this work, including particle size distributions, direct measurement of organic sulfur content and variation, and analysis of stored digital particle images.

ACKNOWLEDGEMENT

The authors would like to acknowledge the support of the U.S. Department of Energy under DOE Contract No. DE-FG02-90ER8079.

REFERENCES

1. Attia, Y.A.; Elzeky, M.; and Ismail, M.; Processing and Utilization of High-Sulfur Coals III, Eds., R. Markuszewski and T.D. Wheelock, 1990, Elsevier, 187 - 196.
2. Helble, J.J.; Srinivasachar, S.; and Boni, A.A.; Idealized Combustion Determination of Ash Particle Formation and Surface Stickiness; Task 8 - Model Development and Integration, Phase I Final Report, U.S. DOE Contract No. DE-AC22-86PC90751, March, 1990, pp.8-1 to 8-195.
3. Huffman, G. P.; Huggins, F. E.; and Dunmyer, G. R.; Fuel, 60 585-597 (1981).
4. Straszheim, W.E.; and Markuzewski, R.; Energy & Fuels 1990, 4, 748-754.
5. Schwoeble, A. J.; Dalley, A. M.; Henderson, B. C.; and Casuccio, G. S.; Journal of Metals, August 1988, pp. 11-14.
6. Casuccio, G. S.; Schwoeble, A. J.; Henderson, B. C.; Lee, R. J.; Hopke, P. K.; Sverdrup, G. M. "The Use of CCSEM and MicroImaging to Study Source/Receptor Relationships." Receptor Models in Air Resources Management, Air Pollution Control Association, Pittsburgh, PA, 1989.
7. Huffman, G.P.; Huggins, F.E.; Shah, N.; and Shah, A.; Prog. in Energy & Combustion Sci., 1990, 16(4), 243-252.
8. Shah, N.; Huffman, G.P.; Huggins, F.E.; Shah, A; Mershon, W.J.; and Casuccio, G. "Graphical Representation of CCSEM Data for Coal Minerals and Ash Particles." To be published in ACS Div. of Fuel Chem. Preprints, Atlanta Meeting, April, 1991.
9. Huffman, G. P.; Huggins, F. E.; Shoenberger, R. A.; Walker, J. S.; Greegor, R. B. and Lytle, F. W.; Fuel 65, 621-632 (1986).
10. Vorres, K.S. Users Handbook for the Argonne Premium Coal Sample Program, Oct. 1, 1989.
11. Samples provided by B.K. Parekh of the University of Kentucky Center for Applied Energy Research.
12. Parekh, B.K.; Groppo, J.G.; Stotts, W.F.; and Bland, A.E.; Column Floatation 88, Chapt. 24, 227-233.
13. Huggins, F. E.; Kosmack, D. A.; Huffman, G. P.; and Lee, R. J.; Scanning Electron Microscopy/1980/I, 531-540, SEM Inc., AMF O'Hare, Chicago, IL 60666, USA.
14. Huggins, F. E.; Huffman, G. P.; and R. J. Lee, ACS Symposium Series No. 205, pp. 239-258, Coal and Coal Products: Analytical Characterization Techniques, Ed., E. L. Fuller, Jr., American Chemical Society, 1982.

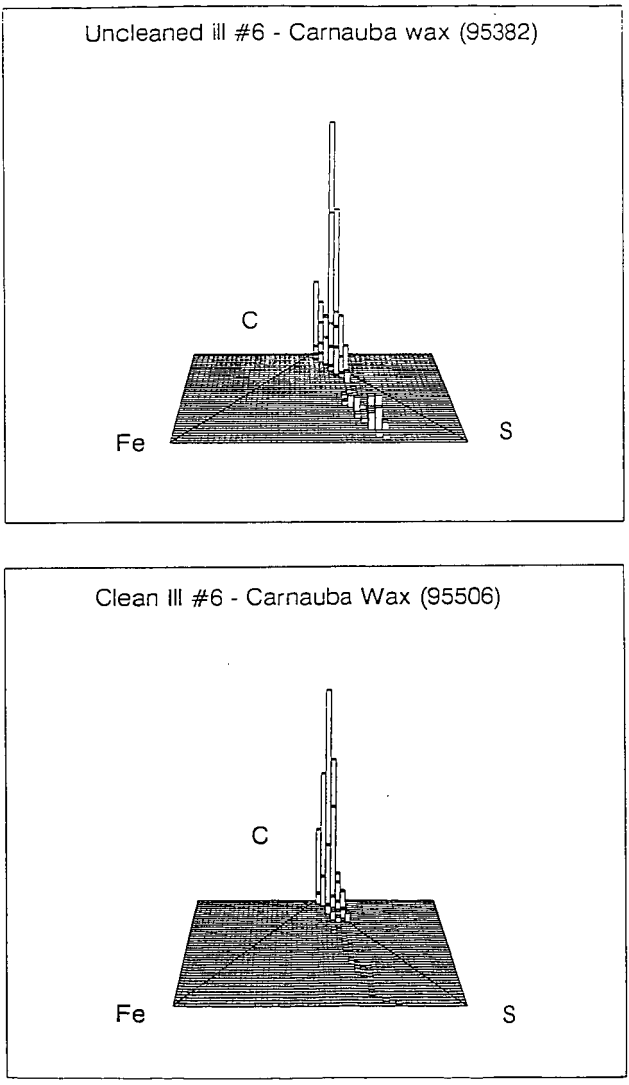

Figure 1. CCSEM number percentage (vertical ordinate) versus composition in a ternary C-Fe-S diagram for raw (top) and cleaned (bottom) Illinois #6 coal mounted in carnauba wax.

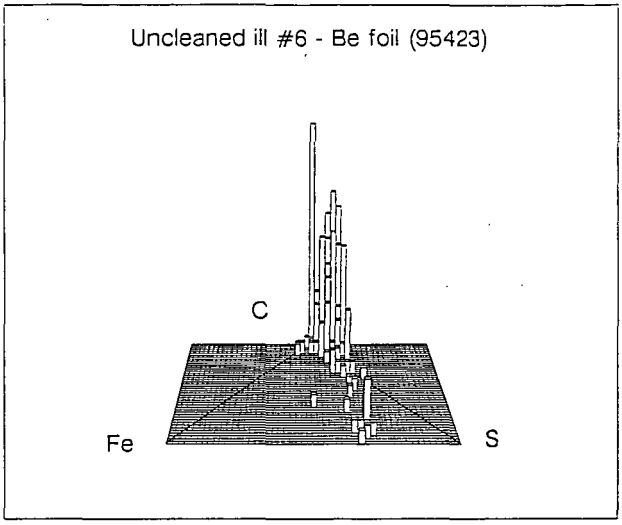

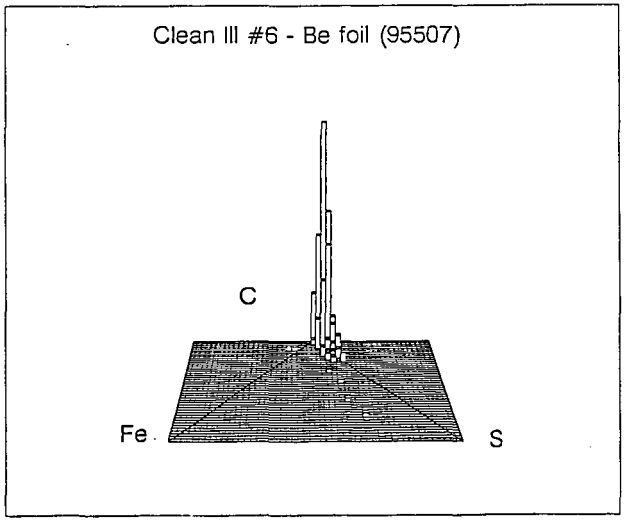

Figure 2. CCSEM number percentage - composition data for raw and cleaned Illinois #6 coal dispersed on beryllium.

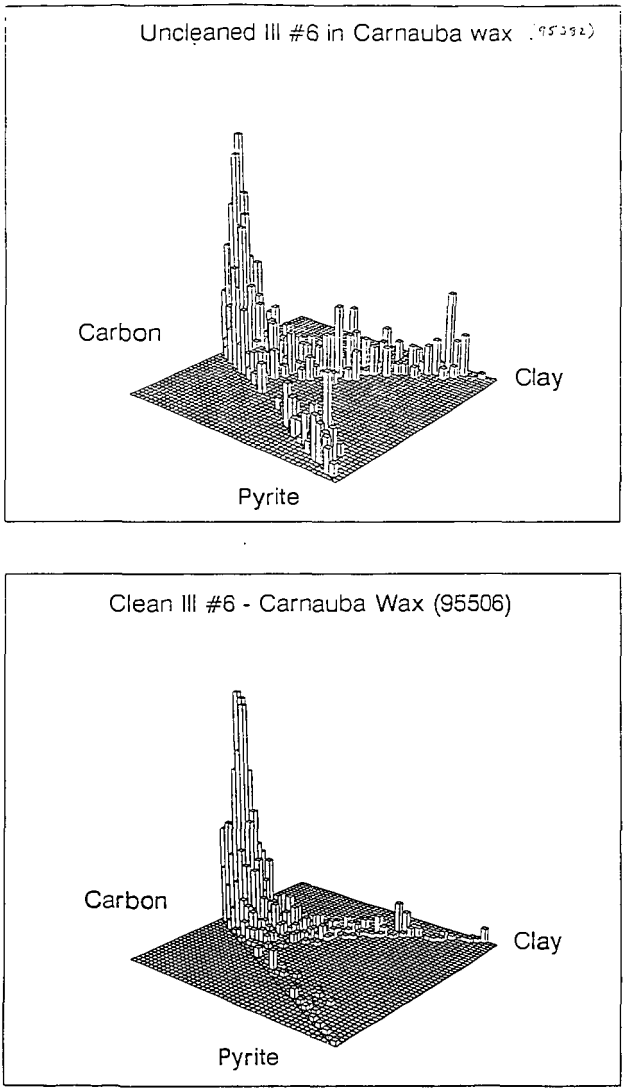

Figure 3. CCSEM number percentage vs. composition in a coal (C) - pyrite (Fe + S) - clay/quartz (Al + Si) diagram for raw (top) and cleaned (bottom) Illinois #6 coal mounted in carnauba wax.

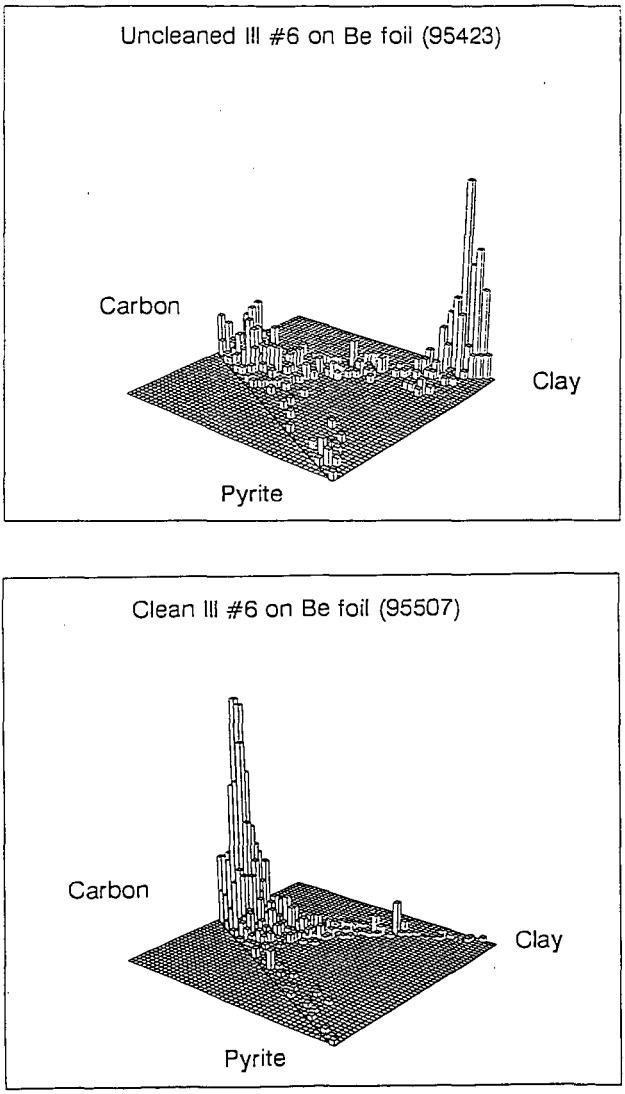

Figure 4. CCSEM number percentage vs. "composition" in a coal-pyrite-quartz/clay diagram for raw (top) and cleaned (bottom) Illinois #6 dispersed on beryllium.

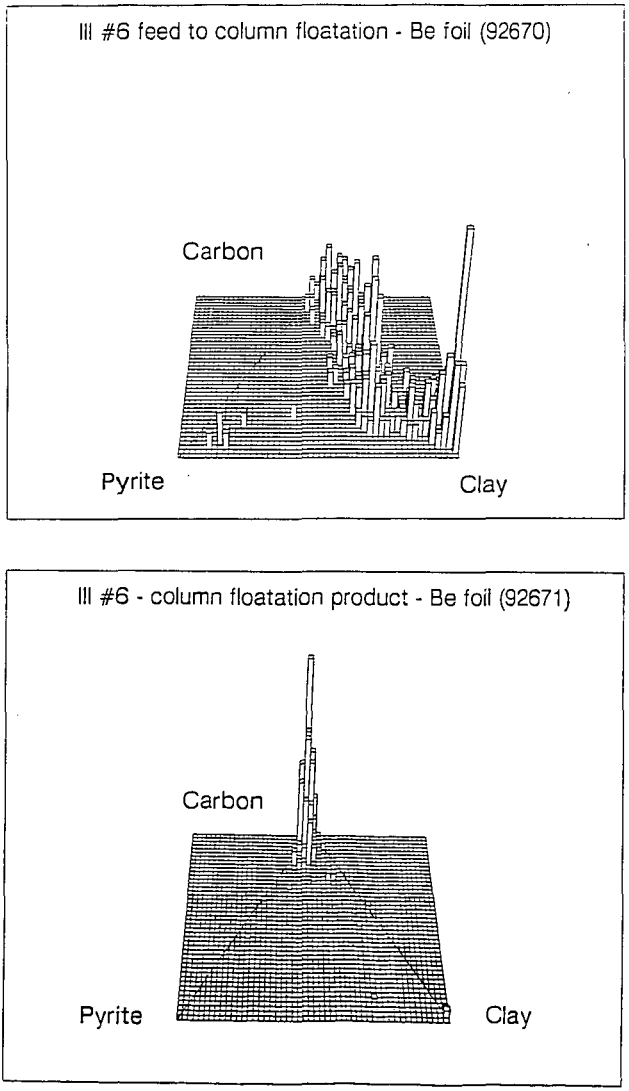

Figure 5. CCSEM number percentage vs. coal-pyrite-clay/quartz composition for Illinois #6 coal before and after column floatation cleaning.

Application of Fluorescence Microscopy to Coal-Derived Resid Characterization

R.F. Rathbone, J.C. Hower and F.J. Derbyshire
Center For Applied Energy Research, Lexington, Kentucky 40511-8433
Keywords: Microscopy, Fluorescence, Resid

INTRODUCTION

This study evaluates the usefulness of a fluorescence microscopy methodology to analyze coal-derived resids and interpret the data in the light of liquefaction processing conditions, process response, the inferred resid reactivity, and in relation to results of other analytical data. The fluorescence technique utilized has been widely applied to coal and kerogen characterization, albeit with some modifications, but is novel in its application to the characterization of coal liquids.

Fluorescence is the emission of light energy which occurs when electrons, having been excited to a higher energy orbital, return to their lower energy ground state. The majority of organic molecules that fluoresce are those with conjugated double bonds (chromophores), such as aromatics, characterised by pi-electrons less strongly bound within the molecule than sigma electrons, that can be excited to anti-bonding pi-orbitals (1,2,3). Increasing the extent of pi-bond conjugation (i.e. larger molecular size) generally imparts a shift in absorption and emission spectra to longer wavelengths. Resid fluorescence largely depends on the concentration and degree of conjugation of aromatic chromophores in the high molecular weight liquids, possibly with ancillary effects from oxygen functionalities. In this context, fluorescence analysis of liquefaction resids can potentially evaluate process performance, since direct liquefaction processes endeavor to break down the macromolecular structure of coal, and reduce the molecular weight of polycondensed aromatics through hydrogenation, the opening of ring structures, and heteroatom removal.

EXPERIMENTAL

Composited Wilsonville CC-ITSL resid samples (combined samples from an entire liquefaction run) received from Consolidation Coal Co., Pittsburgh, PA, consisted of eight non-distillable (at 850°F* or 454°C*) coal liquids (resid) from runs 251-II, 259, 250, and 257. In addition, four pressure filter liquids (PFL) were supplied from the HRI ITSL bench unit, Run I-27 (Table 1). The Wilsonville resids are designated as "interstage" (sampled between the first and second reactor stages) and "recycle" (sampled after the second reactor stage). Samples from HRI Run I-27 are designated with a number representing the sampling day (e.g. PFL P2 = run day 2). Each resid sample was added to several drops of cold setting epoxy resin (with hardener), placed into an epoxy pellet cavity, and allowed to harden. After setting, the sample surface was ground and polished by hand on a rotating lap using a series of grinding papers and alumina polishing compounds.

Fluorescence emission from the resids' polished surface was measured with a Leitz MPV Compact microscope photometer, equipped with a diffraction grating monochromator, a photomultiplier tube, and a 100 W mercury arc lamp (as an excitation source). A Leitz Ploemopak vertical illuminator, housed the necessary filters for ultraviolet-violet (355 to 425nm) illumination, and supported a 50X air immersion objective in the light path. The microscope photometer was interfaced with a computer for data acquisition. Fluorescence spectra were acquired, in argon gas to inhibit photo-oxidation during the analyses, by recording fluorescence intensities every 2.5nm (nominal resolution of 5nm) from 470nm to 700nm. The fluorescence emission from a selected area of resid was scanned 20 times and averaged to get one spectrum per resid particle. Raw spectral data were normalized, a correction factor applied, and then re-normalized so the maximum intensity equaled 100%. The

uncorrected spectra were used to assess fluorescence intensity differences between samples by calculation of the area beneath the spectra. Unlike other chemical analysis methods employed to characterize the liquefaction resids (e.g. refs. 4 & 5), the precision was difficult to evaluate due to inherent variabilities within the Wilsonville resid samples. However, results from replicate fluorescence analyses on the optically homogeneous pressure filter liquids from HRI Run I-27 indicated that fluorescence spectra are repeatable within 3 to 4 nm.

The random reflectance at 546nm off a polished resid surface was obtained utilizing the same microscope photometer employed for fluorescence analysis. A 100 W tungsten-halogen lamp was the illuminant, and isotropic glass standards were used for system calibration. Reflectance analyses were conducted in air immersion because of observed interactions between the resids and microscope immersion oil.

III. Results and Discussion

A. Interstage vs. Recycle Resids

Run 251-II (Wyodak coal, T/C) Fluorescence spectra from the Run 251-II interstage and recycle resid samples are shown in figure 1a, and reveal a shift of the recycle resid fluorescence spectra to shorter wavelengths (spectral "blue shift") compared to the interstage resid. A small, discrete portion of the recycle resid, not shown, displayed a relatively intense yellow fluorescence with an wavelength of maximum intensity (Lmax) of 578 nm. It is possible that it represents one of the three pasting solvent components from the V131B solvent surge tank that was incompatible with the other two components. The mean random reflectance of resids from Run 251-II decreased slightly from the interstage to recycle sample, and, analagous to vitrinite reflectance (6), is considered to represent a decrease in the degree of aromatization and condensation of the recycle resid.

Run 250 (Illinois #6 coal, T/C) A fluorescence spectral "blue shift" and fluorescence intensity increase was recorded for the Run 250 recycle resid compared to its interstage equivalent (Figure 1c). Mean reflectances of the resids decreased by 0.54% from the interstage to recycle sample (Table 1). The difference is significant, as it is greater than 3 standard deviations from the mean values of each sample.

Run 257 (Illinois #6 coal, C/C) Qualitative observations of resid fluorescence revealed substantial variations in these samples, represented quantitatively in figure 1d as two general fluorescence "populations". The origin of this fluorescence variability is not yet known. However, figure 1d does show that, like the Run 251-II and Run 250 resids, the recycle resid fluorescence spectra are at shorter wavelengths than the interstage spectra. The mean resid reflectances from Run 257 decreased by 0.34% from interstage to recycle.

Accompanying the fluorescence "blue shift" of the recycle resids compared to their interstage equivalents, is a decrease in the percentage of aromatic protons, an increase in beta+gamma (≈ aliphatic) protons, and a shift of the phenol peak location to higher wavenumbers (smaller aromatic ring size) in the recycle sample (Table 1). The fluorescence and chemical data from the Run 251-II and 250 resids suggest that the catalytic second stage provided considerable upgrading of resid produced in the thermal liquefaction unit (TLU). This is not unexpected since it is generally considered that the primary role of the first stage TLU is to dissolve the coal (and recycled resid), whereas the second stage upgrades the first stage products (7). Resid from the first stage is derived from the recycle solvent and coal that has been processed for the first time, whereas resid sampled after the second stage catalytic reactor is mainly derived from coal liquids and a much smaller proportion of unreacted coal. It is therefore plausible that the catalytically hydrogenated recycle resid sample displayed a more intense fluorescence, at shorter wavelengths than the interstage sample, indicating the presence of less condensed, lower molecular weight aromatic structures. A similar interpretation is suggested for the Run 257

(catalytic/catalytic) resids: the catalytic second stage has upgraded the products from the catalytic first stage, consistent with the suggestion that some aromatics from the first stage reactor resid product were hydrogenated to less condensed structures.

The selective rejection of preasphaltenes in the critical solvent deasher (CSD) might also have effected the observed fluorescence properties of the Wilsonville resids. A preferential removal of condensed, high molecular weight aromatics can occur in this processing stage, and would contribute to a fluorescence intensity increase and spectral blue shift of the recycle resid.

Run 259 (Pittsburgh coal, C/C) Similarities in the average fluorescence spectra (Figure 1b) and intensities of the interstage and recycle samples suggest that the second catalytic stage in Run 259 did not substantially alter the overall molecular size or concentration of aromatics after the resid had been through a catalytic first stage. The recycle resid exhibited a reflectance slightly lower than that of the interstage sample, although the reflectance values were nearly within one standard deviation of each sample. The minor changes in fluorescence and reflectance properties between the interstage and recycle samples correspond to other chemical properties. The data revealed only a slight decrease of aromatic protons in the recycle sample, and a small increase in beta+gamma proton content.

B. Comparisons Between Wilsonville Runs

The comparisons of the interstage and recycle resid fluorescence properties suggest the spectral distribution and intensity are potential indicators of liquefaction process performance. Strongly bonded high molecular weight condensed aromatic structures, that are likely to be more refractory to upgrading than lower molecular weight less condensed aromatic compounds, would exhibit fluorescence with a low intensity, at comparatively long wavelengths. Conversely, intensely fluorescing resids with spectral distributions at shorter wavelengths are inferred to be relatively reactive to further upgrading.

Interstage Resids The fluorescence spectra of the interstage resids (Figure 2a) suggest the products from Run 259 (Pittsburgh coal, C/C) and Run 251-II (Wyodak coal, T/C) are the least reactive, with relatively low fluorescence intensities, and fluorescence peaks at 700nm or greater. The Run 259 resid is assumed to be comprised of larger, more condensed aromatic structural units than the resid produced in Run 251-II, as indicated by a low fluorescence emission in the 470nm to approximately 600nm region. Proton NMR data indicate the interstage resid from Run 259 has approximately the same percentage of total aromatics as the Run 251-II counterpart, although the latter has relatively more uncondensed aromatics than Run 259 resid. This is not unexpected considering the differences between the two feedstocks: product derived from the subbituminous Wyodak coal is expected to contain smaller, less condensed aromatic structural units than the bituminous-rank Pittsburgh coal. The Run 250 (Illinois #6 coal, T/C) interstage resid has a fluorescence spectrum that is shifted to shorter wavelengths than that of the Run 251-II (Wyodak coal, T/C) or Run 259 (Pittsburgh coal C/C), with an average intensity that is slightly greater than or equal to Run 251-II, but significantly lower than the Run 259 resid. Relative to Run 259, interstage resid from Run 250 was slightly more aromatic (from NMR data in Table 1), contributing to a fluorescence intensity reduction. However, it contains relatively fewer condensed aromatics and more uncondensed aromatics than the interstage resid from Run 259 (hvAb feedstock), probably causing the observed spectral "blue-shift" of the Run 250 resid.

Despite the variability in fluorescence properties of the Run 257 (Illinois #6 coal, C/C) interstage resid (Figure 2a), it is evident that the fluorescence emission of this product is substantially shifted to shorter wavelengths

relative to the other Wilsonville interstage samples investigated. In addition, the total interstage resid composite was substantially less aromatic than the other Wilsonville interstage resids (>10% difference in aromatic protons), with evidence of overall smaller aromatics (phenol peak shifted to higher wavenumbers). The reflectance percent was also significantly lower than the other Wilsonville resids (Table 1), probably due to the lower aromatic content and reduced condensation of the aromatic molecules.

Recycle Resids Between the runs, similar relationships hold for the fluorescence properties of the recycle resids as for their interstage equivalents, figure 2b. As shown in the figure, the average fluorescence spectrum from the Run 251-II (Wyodak coal, T/C) recycle resid was somewhat similar to that from Run 250 (Illinois #6 coal, T/C). Compared to the other Wilsonville resids studied, the Run 257 recycle resid contained the lowest concentration of aromatic protons, while it also had the highest percentage of beta+gamma protons and the phenol peak at a higher wavenumber (3302 cm^{-1}) (Table 1).

C. HRI Run I-27 Resids

The wavelength of maximum intensity (Lmax) of the Run I-27 resids was substantially shifted to longer wavelengths from sample PFL P2 to PFL P18 (Figure 3a), along with a monotonic reduction in relative intensity at the shorter wavelengths, indicating aromatic ring condensation increased as the run progressed. Figure 3b indicates that sample PFL P2 had the greatest average fluorescence intensity, whereas sample PFL P25 had the lowest intensity, suggesting an increased concentration of aromatic chromophores (causing an increase in energy delocalisation) occurred over the course of the run. There was also a progressive increase of resid reflectance from sample PFL P2 to P25. The trends exhibited by the fluorescence and reflectance properties are accompanied by systematic chemical changes. From sample PFL P2 to P25, there is a monotonic increase in percent aromatics, a decrease in beta+gamma proton concentrations, and a shift in phenol peak frequency from 3305 to 3296 cm^{-1} (Table 1), indicative of increasing ring condensation.

The fluorescence "red-shift", intensity decrease, and increase in resid reflectance percent over the course of Run I-27 suggest that, with an increase in age, the catalyst became less effective in upgrading the non-distillable fraction of coal liquids to low molecular weight, less aromatic products as aromatic ring hydrogenation became less pronounced during the run. A possible cause of these deleterious changes in resid properties over the course of the run is the partial deactivation of catalyst from deposition of carbonaceous materials onto the catalyst surface, which is believed to occur most rapidly in the early stages of the liquefaction run (8). Other process variables that may have influenced resid fluorescence and chemical properties include increased reactor temperatures, a solvent/coal ratio reduction, and an increase in the solvent cut-point (9).

VI. Summary and Conclusions

Quantitative fluorescence microscopy is potentially a rapid, inexpensive technique which can provide new insight into the structure and composition of coal-derived resid, and could lead to more effective process control. Perhaps the greatest strength of quantitative fluorescence microscopy is its ability to resolve inhomogeneities within coal-derived resid samples, including, but not limited to, minerals, unreacted macerals, and multiple resid phases. This capability is not possible with most other analytical techniques which typically require resid dissolution in a solvent prior to analysis. Whereas these analytical techniques provide chemical and structural information on a homogenized resid sample, and only on the soluble portion, inherent variability within the coal liquids can be identified and measured with fluorescence microscopical methods.

Acknowledgements

This work was supported by subcontract from Consolidation Coal Co. under U.S. Department of Energy Contract No. DE-AC22-89PC89883.

VII. References

(1) Bridges, J.W., In Luminescence in Chemistry (Ed. E.J. Bowen), D. Van Nostrand Co., 1968, pp. 77-115.
(2) Wehry, E.L., In Fluorescence: Theory, Instrumentation and Practice (Ed. G.G.Guilbault), Marcel Dekker, 1967, pp. 37-132.
(3) George, G., In Luminescence Techniques in Solid State Polymer Research (Ed. L. Zlatkevich), Marcel Dekker, 1989, 318 pp.
(4) Robbins, G.A., Winschel, R.A. and Burke, F.P., Am. Chem. Soc. Div. Fuel Chem.Prepr., 1985, 30(4), pp. 155-163.
(5) Winschel, R.A., Robbins, G.A. and Burke, F.P., Fuel, 1986, 65, pp. 526-532.
(6) McCartney J.T. and Teichmuller, M., Fuel, 1972, 51, pp. 64-68.
(7) Derbyshire, F.J., Varghese, P. and Whitehurst, D.D., Fuel, 1983, 62, pp. 491-497.
(8) Derbyshire, F.J., Catalysis in Coal Liquefaction: New Directions for Research, IEA Coal Research, 1988, 69 pp.
(9) Consolidation Coal Co., personal communication to authors.

Table 1

Run No.	Coal	Sample[1] Type	Proton NMR Data[2] Arom. (%)	Bet+Gam (%)	Peak[3] (cm^{-1})	Reflectance[4] (%)	s.d.
251-II	Wyodak	T/C, Int	33.2	37.6	3294	7.80	0.22
251-II	Wyodak	T/C, Rec	26.8	44.8	3298	7.66	0.25
259	Pittsburgh	C/C, Int	33.3	35.6	-	7.82	0.11
259	Pittsburgh	C/C, Rec	31.5	40.2	-	7.70	0.26
250	Illinois #6	T/C, Int	34.5	35.3	3292	7.84	0.13
250	Illinois #6	T/C, Rec	26.1	45.2	3299	7.30	0.15
257	Illinois #6	C/C, Int	21.8	49.5	3300	6.82	0.20
257	Illinois #6	C/C, Rec	19.9	52.0	3302	6.48	0.19
I-27	Illinois #6	C/C, Day 2	14.5	57.3	3305	6.21	0.12
I-27	Illinois #6	C/C, Day 8	20.7	51.0	3301	6.80	0.07
I-27	Illinois #6	C/C, Day 18	29.2	40.5	3297	7.57	0.14
I-27	Illinois #6	C/C, Day 25	38.3	32.8	3296	8.06	0.08

1. T/C = thermal/catalytic, C/C = catalytic/catalytic, Int = interstage resid, Rec = recycle resid
2. Arom. = aromatic protons, Bet+Gam = beta and gamma protons (ref. 5)
3. Peak = FTIR phenol peak location (see ref. 4)
4. (%) = mean reflectance %, s.d. = standard deviation

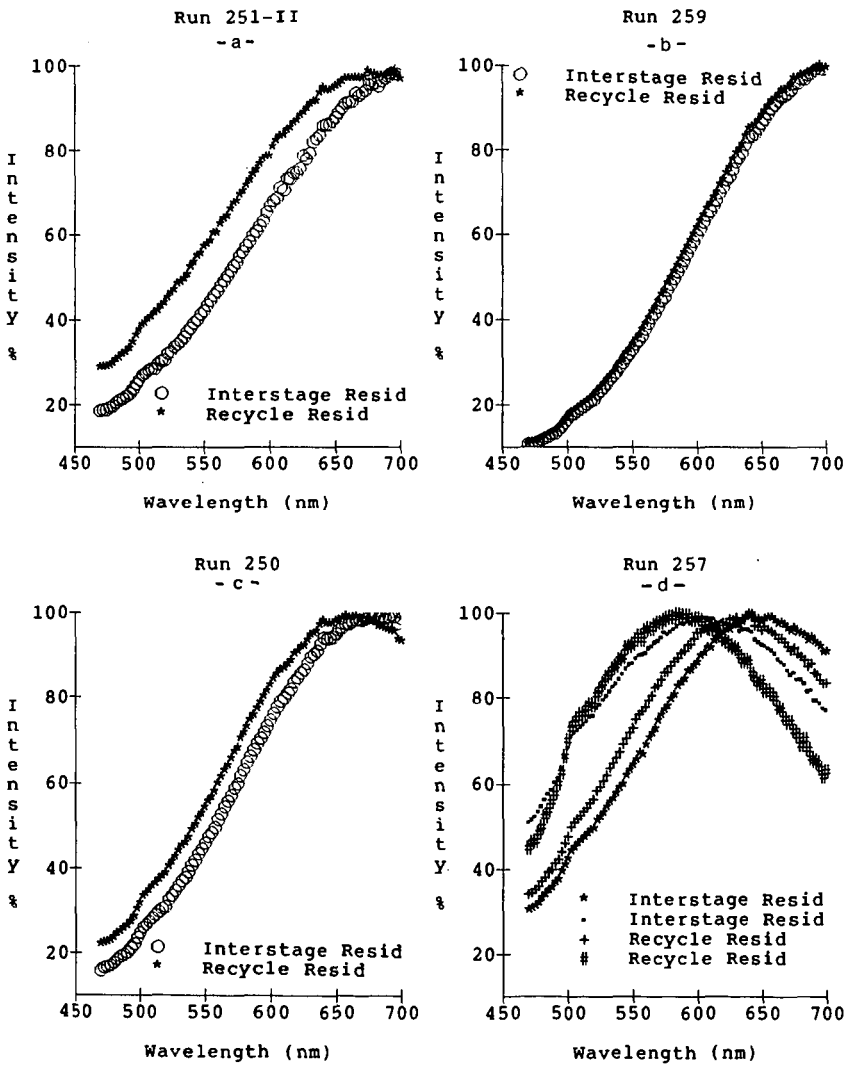

Figure 1. Corrected fluorescence spectra of resids from Run 251-II (a), Run 259 (b), Run 250 (c), and Run 257 (d). Data for each resid sample represent the average of five spectra.

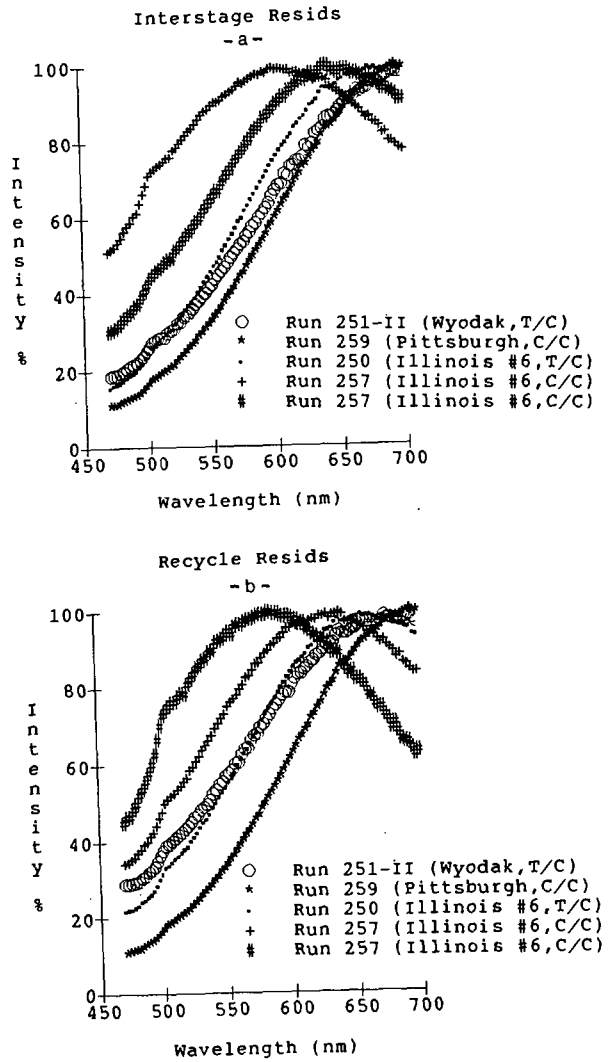

Figure 2. Corrected fluorescence spectra for the Wilsonville interstage (a) and recycle (b) resids. Data for each resid sample represent the average of five spectra.

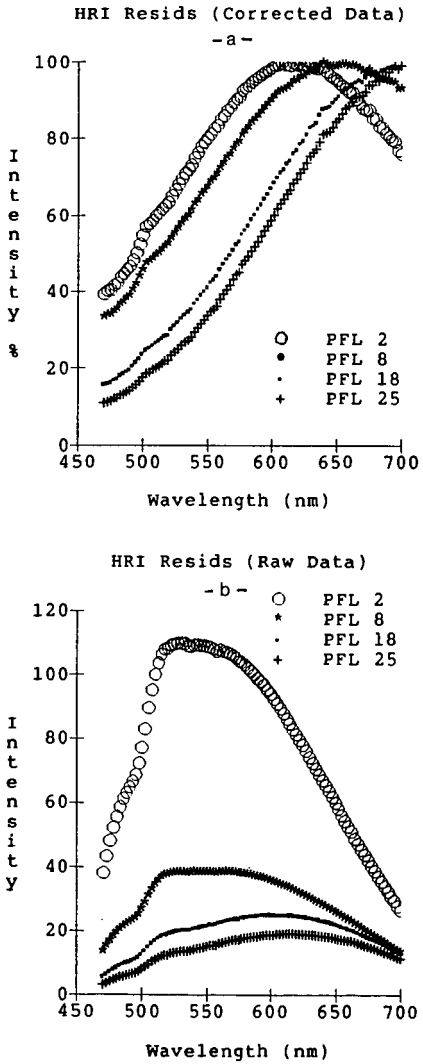

Figure 3. Corrected (a) and uncorrected (b) fluorescence spectra for HRI Run I-27 PFL resids. Data for each resid sample represent the average of five spectra.

THE APPLICATION OF ADVANCED ANALYTICAL TECHNIQUES TO DIRECT COAL LIQUEFACTION

Susan D. Brandes, Richard A. Winschel, Francis P. Burke
CONSOLIDATION COAL COMPANY
Research & Development
4000 Brownsville Road
Library, PA 15129

Keywords: Liquefaction, Analytical Techniques

INTRODUCTION

Direct coal liquefaction is a complicated and ill-defined chemical process. In order to promote coal liquefaction as a feasible alternative-energy technology, fundamental chemical understanding of the direct liquefaction process must be obtained. There exists, however, a gap between the advanced, modern techniques of the analytical chemist and the application of those techniques by the direct coal liquefaction process developer. There are two major reasons for the existence of this gap: 1) Much research in advanced analytical chemistry concentrates on instrument development and not method application, and 2) appropriate direct coal liquefaction samples for method applications are frequently difficult to obtain.

Consol is coordinating a program designed to bridge the gap, and thus to advance our knowledge of the process chemistry of direct coal liquefaction. The program is designed to provide well-documented samples to researchers who are utilizing techniques potentially useful for the analysis of coal derived samples. The choice of samples and techniques was based on an extensive survey (1) made by Consol of the present status of analytical methodology associated with direct coal liquefaction technology. Sources of information included process developers and analytical chemists.

Identified in the survey are a number of broadly characterizable needs. These categories include a need for:

- a better understanding of the nature of the high molecular weight, non-distillable residual materials (both soluble and insoluble) in the process streams.
- improved techniques for molecular characterization, heteroatom and hydrogen speciation and a knowledge of the hydrocarbon structural changes across coal liquefaction systems.
- better methods for sample separation.
- application of advanced data analysis methods.
- the use of more advanced predictive models.
- on-line analytical techniques.
- better methods for catalyst monitoring.

Various analytical techniques currently in routine use provide a valuable, but incomplete, understanding of direct coal liquefaction process chemistry, and thus cannot fully address these needs. In this program, specific methodologies (or

techniques) potentially relevant to addressing some of these needs have been identified (Table 1). Many of these methods are new only in that they have not been fully demonstrated for their applicability to coal liquids. Other techniques are "cutting edge" and are currently under development for a number of applications, including natural product analyses. Organizations or research groups that are involved in the program are identified, in Table 1, with the method that they are employing.

Methods under consideration in this program are directed towards the characterization of the non-distillable resid portion of liquefaction oils because of the importance of this material to the liquefaction process. In current direct liquefaction technology, the heaviest soluble materials produced from the coal are recycled to near extinction. These heavy soluble materials (850°F+) typically account for 50% of the recycle stream fed to the first reactor stage in current U.S. two-stage liquefaction technology. At a 2:1 recycle stream to coal feed ratio to the first stage, the principal reactor feedstock is recycled resid, not coal. The analysis of this heaviest portion of the direct liquefaction product stream (the resid) is a much more challenging problem than analysis of the lighter materials produced by coal liquefaction. It is believed that by understanding the composition and behavior of this heavy material an improved understanding of the direct coal liquefaction process will be achieved.

PROGRAM STRUCTURE

In order to bridge the gap between the process developer and the analytical chemist and improve our fundamental understanding of the chemistry of coal conversion to liquid products, a program was organized by Consol to coordinate the distribution of well-documented direct coal liquefaction samples to evaluate potentially useful analytical techniques. The results are being evaluated in regard to the usefulness of the analytical information in adding to the chemical knowledge of the direct liquefaction process. The program is structured into two phases. In Phase I, a number of organizations were chosen to participate in the program (Table 1). Eighteen different analytical methods were incorporated into the program for Phase I. These methods are, for the most part, well established analytical techniques which are uncommon in their application to coal-derived materials. Each researcher is responsible for the interpretation of the results of the tests in light of the processing information provided by Consol with each sample. In order to provide the maximum information on any one sample, Phase I of the program was structured to use techniques which both complement and supplement each other. Phase II of the program may include expansion of Phase I tests with methods that appear to be promising, the addition of methods and techniques not considered in Phase I, and a concerted effort to tie together the methods which were chosen in Phase I. Phase II also will be the appropriate point in the program to evaluate the reliability of the analytical information from promising techniques. This may be accomplished, when practical, by round robin tests.

SAMPLES

A key to the success of the program is the proper selection of samples. Evaluation of the analytical methodologies will be based in part on the utility of the method for identifying differences in the samples which can be attributed to differences in the conditions under which the samples were produced. This may include such diverse variables as feed coal rank, reactor temperature, catalyst type, age, or use in one or both reactors (in a two-stage system), sampling point in the direct coal liquefaction plant, and whether or not the feed coal was in some way treated before liquefaction. It is necessary to provide a diverse set of samples to the analytical researcher for testing. In Phase I of the program, sample sets for each method were

chosen with large differences in production variables (Table 2). Analytical methods that cannot only distinguish among the samples, but can provide information useful for predictive purposes will be considered successful techniques.

All samples in the program come from the Consol sample bank, which includes materials from the Wilsonville, Lummus, HRI, H-Coal Pilot Plant, and UOP liquefaction and coprocessing programs. In addition, Consol continues to obtain and analyze samples from active DOE-sponsored process development programs. All samples distributed in the program were analyzed by Consol. Such analyses include (when appropriate): elemental analysis, ash content, ash elemental analysis, solubility fractionation, phenolic -OH concentration, calorific value, and hydrogen classes by ^{1}H-NMR. In addition, Consol has documented the full history of the samples (plant, process conditions, age, storage conditions, hydrogen consumption, and yield data for the associated run). Kinetic parameters were calculated for a number of the coal liquefaction runs from which samples were selected for the program. All information was supplied to the program participants to aid in the evaluation of the analytical methods.

The sample sets for the entire program were integrated so that the maximum information content can be obtained not only by judicious choice of samples for analysis by any one method, but by the application of as many of the methods as possible to a single sample. A total of eighteen different methods will be utilized in Phase I of the program. Some of these methods, for example Field Ionization Mass Spectrometry and Field Desorption Mass Spectrometry, will be used for identical samples and will yield similar information. In other cases, different analyses will provide a better understanding of the sample, for example: the use of carbonization tests to determine the propensity of the process oil to undergo retrogressive reactions will be supplemented with information on the chemical content of that oil obtained by separation technologies, such as supercritical fluid chromatography. Numerous other examples of integration of the methods exist in the program. These become apparent by examination of Table 1.

ANALYTICAL METHODOLOGIES

The analytical methodologies employed in the program are most easily discussed by categorizing them with the needs that they address. The research groups or organizations that are investigating the use of these techniques are identified in the following text; more detail can be found in Table 1.

Resid Analysis

Resids will be inspected by microscopic techniques. The Pennsylvania State University will study samples with reflectance techniques, the University of Kentucky Center for Applied Energy Research will use fluorescence techniques. Changes in reflectance of certain macerals can indicate if the material has undergone forward reaction (hydrogenation) or retrogressive reaction (condensation). Chemical analysis of resids will include various separation techniques, specifically liquid chromatography (LC), supercritical fluid chromatography (SFC), and solubility fractionation. Supercritical fluid chromatography will be employed by Virginia Polytechnic Institute to study higher molecular weight materials with limited volatility. Coupled with mass spectrometry, SFC is a powerful technique for the examination of materials with molecular weights in excess of 600 Daltons. The National Institute for Petroleum and Energy Research will use a methodology for the separation of resids into more tractable fractions for further analysis by separation based on solubility fractionation, acid/base/neutral separations, and separations based on functionality. Analysis of the resulting fractions will simplify the correlation of the behavior of the material to the process conditions.

Two potential spectroscopic techniques for resid analysis are infrared or Fourier transform infrared (FTIR) spectroscopy and mass spectrometry (both field ionization mass spectrometry (FIMS) and field desorption mass spectrometry (FDMS)). The combination of FTIR with thermogravimetric analyses (TG-FTIR), which will be done by Advanced Fuel Research, allows for the rapid spectral identification of the components of the thermally evolved material. The char remaining in the TG is subsequently burned in oxygen and CO_2, H_2O, and SO_2 are measured. Battelle PNL will employ field desorption mass spectrometry (FDMS) as another technique suitable for the direct analysis of resids. Using ionization modes such as field desorption (FD), high molecular weight samples can be ionized directly from the condensed phase without the need for vaporization by heating. SRI international will utilize FIMS (field ionization mass spectrometry) which has an advantage over other methods of ionization in that it produces molecular ions in high abundance with fragmentation occurring only rarely; thus a molecular weight profile of the material is obtained with reasonable clarity and accuracy.

Heteroatom Speciation

One of the most important problems associated with the analytical work on coal liquids is that of being able to follow and identify the heteroatom species through the process, from the feed coal to the various product streams. Determination of the functional groups important for retrograde reactions and resid reactivity is considered of paramount importance. The most difficult to detect and measure directly are the oxygenated species. A method which will be used by SRI International to attempt to track some of the oxygenated species is trimethyliodosilane derivatization. The method is a wet chemical technique for partial analysis of the oxygen functional groups in coal-derived resids. It involves the reaction of $(CH_3)_3SiI$ with alkyl carbon-oxygen bonds (ROR', ROAr, RCOOR', RCOR', RCOH, and ROH) to produce alkyl carbon-iodine bonds. Sulfoxides also react, though this is not an expected group in coal liquids. Alkyl carbon-oxygen bonds are quantified by measuring reacted iodine. A more direct technique which will be employed by Advanced Fuel Research to determine the concentration of hydroxyl groups is quantitative Fourier transform infrared spectroscopy (FTIR). In addition, qualitative analysis of the resid material by FTIR may yield information on the types of ether linkages present (oxygen linked to aliphatic or aromatic carbon).

Hydrogen Speciation and Hydrocarbon Structure

Tracking of the hydrogen in the coal liquefaction system is a formidable task. One technique which will be examined by Western Research Institute for estimation of the hydrogen consumed in hydrogenation and bond cleavage reactions, and heteroatom removal, is based on both ^1H and ^{13}C solid-state NMR. Solid-state NMR measurements can be made on whole coals, resids, and insoluble fractions obtained at different stages in the liquefaction process, and from different liquefaction processes. Two-dimensional NMR will also be applied to coal samples by Battelle PNL. A second technique which will be applied to both resids and distillates by Advanced Fuel Research is FTIR. Determination can be made of the distribution of aromatic hydrogen (whether 1, 2 or more adjacent hydrogens are on a ring), and the forms of aliphatic hydrogen (methyl, or methylene).

On-line Analyses

Methodologies for on-line analysis of liquefaction process streams are difficult to formulate. Techniques which rely on optical throughput or scattering often are not amenable to materials which are opaque or contain particulate matter. One method with some potential is FTIR. This technique has not yet been applied to coal liquefaction process streams, although it has proven useful for on-line stability measurements of jet fuels. Preliminary scoping studies by Advanced Fuel Research will show if the method is feasible.

Application of Standard Petroleum Feed Tests to Coal Liquefaction Products

A definite analytical need of the processor of coal liquefaction products is to know the refining requirements of the raw liquid products. A correlation drawn between operating variables of the finishing process and net product characteristics (in regard to specification requirements) will be extremely useful. In addition, this knowledge will provide more accurate estimations of upgrading costs to specification fuels. Although it is acknowledged that the standard petroleum feedstock tests are not tailored for the analysis of coal liquids, it is believed that they are at least a starting point for this analysis. Therefore, in a directed attempt to meet this particular analytical need, standard petroleum refinery feed analyses were performed by Conoco, Petroleum Products Research Division, on products of the Wilsonville plant.

CONCLUSION

The goal of this work is to bridge the gap between the analytical chemist and the direct coal liquefaction process developer by identifying, demonstrating, and verifying the usefulness of novel analytical techniques for the analysis of direct coal liquefaction derived materials. As described above, this program successfully matches these analytical needs and the novel analytical technologies.

ACKNOWLEDGEMENTS

This work is funded by the U.S. Dept. of Energy under contract No.DE-AC22-89PC89883

REFERENCES

1. Brandes, S.D.; Robbins, G.A.; Winschel, R.A.; Burke, F.P. "Coal Liquefaction Process Streams Characterization and Evaluation - Analytical Needs Assessment, Topical Report"; DOE Contract No. DE-AC22-89PC89883, March 1991.

TABLE 1

ANALYTICAL METHODOLOGIES

Organization Analytical Method	Samples	Variables
SRI International		
Field Ionization Mass Spectrometry (FIMS)	Distillation Resids (850°F⁺)	Coal Rank Reactor Configiguration Sampling Point
Oxygen Speciation by Derivatization	Whole Process Oils	Coal Rank Thermal Pretreatment
Battelle PNL		
2-D NMR spectroscopy	Distillation Resids (850°F⁺) Feed Coals	Coal Rank Sampling Point
Field Desorption Mass Spectrometry (FDMS)	Distillation Resids (850°F⁺)	Coal Rank Reactor Configuration Sampling Point
Supercritical Fluid Chromatography (SFC)	THF-Soluble Portion of Distillate Resids	Coal Rank Reactor Configuration Sampling Point
The Pennsylvania State University		
Gold Tube Carbonization	Distillation Resids (850°F⁺)	Coal Rank Reactor Configuration Sampling Point Thermal Pretreatment
Reflectance Microscopy	THF-Insoluble Resids	Coal Rank Reactor Configuration
Advanced Fuel Research		
FTIR	Distillation Resids (850°F⁺) THF-Soluble Portion of Distillate Resids	Coal Rank Sampling Point Catalyst Age
TG-FTIR	Distillation Resids (850°F⁺) THF-Soluble Portion of Distillate Resids	Coal Rank Sampling Point

TABLE 1 (Cont'd)

ANALYTICAL METHODOLOGIES

Organization Analytical Method	Samples	Variables
University of Kentucky/Center for Applied Energy Research		
Fluorescence Microscopy	Distillation Resids (850°F⁺) THF-Soluble Portion of Distillate Resids	Coal Rank Sampling Point Catalyst Age
Virginia Polytechnic Institute		
LC-FTIR • Sampling Point	THF-Soluble Portion of Distillate Resids	Coal Rank Reactor Configuration Ashy/Deashed Streams
SFE-SFC • Sampling Point	THF-Soluble Portion of Distillate Resids	Coal Rank Reactor Configuration Ashy/Deashed Streams
Western Research Institute		
Solid State $^{1}H/^{13}C$ NMR	Distillation Resids (850°F⁺)	Coal Rank Sampling Point
^{13}C NMR	Process Oils	Coal Rank Sampling Point
National Institute for Petroleum and Energy Research		
Acid/Base/Neutral Separation	Distillation Resids (850°F⁺)	Coal Rank Sampling Point
High-Performance Liquid Chromatography (HPLC)	Filter Liquids Process Oils	Pretreatment Coal Cleaning
2-D NMR	Distillation Resids (850°F⁺) Process Oils	Coal Rank Sampling Point
Conoco Inc., Petroleum Products Research Division		
ASTM Crude Oil Analyses	Net Product Oil	Coal Rank

TABLE 2

PROGRAM SAMPLE SET

Wilsonville Pilot Plant Samples

850°F+ Distillation Resid Samples
Runs: 250, 251, 257, 259, 255, 256, 257
Sample Streams: Recycle, Interstage, Second Stage Product

Tetrahydrofuran Insoluble of 850°F+ Distillation Resids
Runs: 250, 251, 257, 259
Sample Streams: Recycle, Interstage

Tetrahydrofuran Soluble Portion of 850°F+ Distillation Resids
Runs: 250, 251, 256, 257, 259, 260
Sample Streams: Recycle, Interstage, Second Stage Product

Whole Oil Samples
Runs: 251, 255, 257, 259
Sample Streams: Recycle, Interstage, Second Stage Product, Net Overhead Products

THF Soluble Portion of Whole Oil Samples
Run: 259
Sample Stream: Recycle

HRI Bench Unit Samples

850°F+ Distillation Resid Samples
Runs: I-27, CC-2, CC-5
Sample Streams: Pressure Filter Liquid, First Stage Process Oil
Tetrahydrofuran Portion of 850°F+ Distillation Resids
Runs: CC-2, CC-5
Sample Streams: Pressure Filter Liquid, First Stage Process Oil
Whole Oil Samples
Runs: CC-1, CC-2, CC-5
Sample Streams: Pressure Filter Liquid, First Stage Process Oil, Separator Process Overhead Distillate

Lummus Process Development Unit

850°F+ Oistillation Resid Samples
Run: 3LCF10
Sample Stream: Feed to LC-Finer

Tetrahydrofuran Soluble Portion of 850°F+ Distillation Resids
Run: 3LCF10
Sample Stream: Feed to LC-Finer

DETERMINATION OF ORGANIC/INORGANIC ASSOCIATIONS OF TRACE ELEMENTS IN AN OIL SHALE KEROGEN

Gregory E. Mercer, Scot Fitzgerald, Jeffrey Day and Royston H. Filby
Department of Chemistry
Washington State University
Pullman, WA 99164-4630

INTRODUCTION

The distributions of trace element in crude oils have been used to classify crude oils into families (1-4). Relatively little work, however, has been performed using trace element abundances for oil-source rock correlations. One reason for the paucity of oil-source rock correlations using trace elements is the difficulty in obtaining accurate trace element data for the organic matter (bitumen and kerogen) found in source rocks. The most difficult problem is the determination of trace element abundances in kerogens which are the precursors to crude oils. The chemical species of metals present in kerogens must be known to provide the relationship between such species and the metal complexes in crude oils. Difficulties in kerogen analysis arise primarily from the method of isolation, i.e., dissolution of the mineral matrix of the rock. In the conventional method of isolation the mineral matrix is dissolved in HCl/HF. This leaves a kerogen containing HCl/HF resistant minerals and neoformed fluorides. Several methods to remove or account for these inorganic contributions to the kerogen composition have been proposed, and include low temperature ashing (LTA) (5), density separations (6) and chemical removal of residual mineral matter (7-9). Although most of these methods improve trace element data, they have drawbacks; for example, density separations are usually incomplete (7) and chemical removal techniques do not dissolve the major resistant minerals without seriously altering the organic matter. The LTA method which is based on low temperature oxidation of organic matter to CO_2 + H_2O and conversion of organically combined metals to acid-soluble oxides is affected by the presence of neoformed fluorides and by partial oxidation of pyrite/marcasite (11).

This paper compares two methods of determining inorganic/organic trace element abundances in kerogen with the LTA method developed previously (11). A combination of INAA with X-ray diffraction analysis and analysis of mineral grains by electron microprobe (EMP-XRF) was used to analyze density fractions of the New Albany Shale kerogen and a mineral-rich fraction of the kerogen. The New Albany kerogen was chosen because of the large Ni and V concentrations and because of the high metalloporphyrin concentrations in the shale (12).

EXPERIMENTAL

1. Kerogen Isolation. Mississippian New Albany shale (Henryville Bed Clark County, IN) was ground to ~200 mesh in a ring mill, washed with distilled water and vacuum dried at 65°C. Resultant shale samples were extracted with toluene-methanol (7:3) to remove bitumen and demineralized as indicated in Figure 1. Detailed geological information on New Albany shale may be found elsewhere (10).

2. Density Separations. A kerogen sample isolated using the scheme shown in Figure 1 were subjected to a density fractionation using chloroform. In this separation the kerogen was sonicated in chloroform at 40°C for an hour and centrifuged. Roughly 80% of the kerogen was recovered in a float fraction, 15% as a sink fraction and ca. 1% as a mineral residue which was approximately 85% pyrite and marcasite. A portion of the mineral residue was treated with 3M nitric acid at 45°C for one hour to remove the pyrite and marcasite from minor mineral components, (e.g., rutile, chalcopyrite, anatase, etc.).

3. Instrumental Neutron Activation Analysis (INAA). All samples were analyzed for trace element contents by INAA using a method similar to that of Jacobs and Filby (13).

4. X-ray Diffraction (XRD). the major mineral composition of the samples was determined by XRD using a Siemens x-ray diffractometer. Appropriate portions of each powdered sample were smeared on a glass slide and diffraction patterns measured using the Cu-K_α line.

5. Electron Microprobe X-ray Fluorescence (EMP-XRF). Trace element associations with individual mineral grains within the kerogen were determined by EMP-XRF. Electron dot maps of several elements in ashed kerogen were made using a Cameca electron microprobe. The microprobe was also used in the SEM mode to obtain electron micrographs of the mapped mineral grins. For both electron dot maps and micrographs an electron accelerating voltage of 20keV was used. Concentrations of several elements in individual mineral grains were also determined.

6. Low Temperature Ashing (LTA). Kerogen samples were ashed using a LFE Model LTA-302 low temperature asher operated at 50 RF watts and an O_2 flow rate of 2 mL/min. Ashed samples were treated with 2M HCl and heated to 40°C with constant stirring for one hour to remove metal oxides formed in the ashing process. The acid-leached ash was isolated by centrifugation.

RESULTS AND DISCUSSION

1. X-ray Diffraction Results

The major minerals identified by XRD in New Albany kerogen were pyrite and marcasite. Additional minor mineral components were identified by ashing the kerogen followed by removal of the pyrite and marcasite from the mineral residue with 3M HNO_3. In the ashed kerogen ralstonite ($NaMgAl(F,OH)_6.nH_2O$) was identified. This mineral is an artifact of the kerogen isolation procedure as discussed elsewhere (5,11). Leaching of the ash with 3M HNO_3 removed ralstonite, pyrite and marcasite and XRD identified anatase, rutile and chalcopyrite ($CuFeS_2$). With these inorganic contributions revealed, correction methods were focused on the minerals identified above.

2. Fractionation of Kerogen by Density: Determination of Concentrations in Inorganic and Organic Components.

The concentrations of trace elements determined by INAA for the kerogen and its density fractions are listed in Table 1. A number

of general conclusions concerning the inorganic/organic nature of trace elements in the kerogen may be drawn from the data. Elements which tend to concentrate in the float fraction (Ni, V, Mo, Sb) probably have high organic associations. Similarly, elements concentrating in the most dense fraction, the mineral residue (As, Cr, Fe, Hf, Mn, Ti, Zr) most likely are present predominantly in mineral form. The elements which concentrate in the intermediate density sink fraction (Al, Mg, Na, Cs, Rb, Sc) appear to be associated with neoformed fluorides, such as ralstonite. However, some elements show no appreciable concentration in any fraction (Co, Se) and possibly exist in both inorganic and organic forms in the kerogen.

A method to determine the concentrations of the elements in the "organic" and "inorganic" compounds was formulated based upon the weight fractions of the organic and inorganic components. In this method the following assumptions are made:

1) The mineral matter and organic matter are similar in the float and sink fractions. The fractions differ only in the relative amounts of organic and mineral matter.

2) The concentration of V in organic combination is very large relative to the V in inorganic combination.

3) The concentration of Fe in inorganic combination is very large relative to the Fe in organic combination.

Using these assumptions, the inorganic and organic weight fractions for the sink and float kerogen samples were determined as shown in Figure 2. Once the weight fractions (f_{1O}, f_{1m}; f_{2O}, f_{2m}) are known, the concentration of any element may be determined for both the organic and inorganic components of kerogen by solving the two simultaneous equations shown at the bottom of Figure 2. The trace element concentrations in the "organic" and "inorganic" components of the original kerogen, as determined by this method, are listed in Table 2.

3. Determination of Organic and Inorganic Associations by Analysis of the Mineral Residue.

Pyrite and marcasite were the only minerals identifiable by XRD in the mineral residue. After removal of pyrite and marcasite with HNO_3, however, the XRD pattern confirmed the presence of chalcopyrite, rutile and anatase as minor mineral components in the kerogen. The trace element concentrations in the mineral residue before and after the HNO_3 treatment are shown in Table 3 and confirm the XRD data. A number of elements (e.g., As, Co, Fe, Mn, Mo, Ni, S, and Sb) are 90-100% leached by $3MHNO_3$. These elements are thus associated with pyrite, marcasite or other minerals which are soluble in dilute HNO_3 (but not in HCl/HF). As a result, the inorganic associations for these elements in the kerogen may be accounted for based upon their dissolution in the HNO_3 relative to the dissolution of Fe. The assumptions made in this method for estimating mineral associations are as follows:

1) The mineral residue is representative of the inorganic component of the original kerogen. This will not be true for neoformed fluorides (e.g., ralstonite).

2) The fraction of Fe in organic form in the kerogen is small.

3) The amount of an element dissolved is proportional to the amount of Fe dissolved. This will not be the case for elements associated with ralstonite (Na, Mg, Al, etc.).

This technique is limited to elements which form sulfides but may be more reliable for most of these elements than the density fractions method as a result of the basic assumptions behind each method. A correction for Se, however, cannot be made due to the formation of elemental S (and hence elemental Se) during the pyrite dissolution. The data for Cu in Table 3 indicate that roughly 4% of the sulfur in the HNO_3-treated mineral residue sample is in the form of chalcopyrite leaving ~20% of the sample as elemental S. Thus, the true inorganic Se content would be underestimated in this "pyrite dissolution method" because of the chemical similarities between S and Se, i.e., oxidation of H_2Se to Se^o by HNO_3 would occur. The inorganic contributions to the original kerogen trace element content, as determined by this method, are listed for several elements in Table 4 (see also Table 2).

4. EMP-XRF Analysis. Electron micrographs and elemental distributions of the ashed kerogen indicate that both framboidal and massive type pyrite/marcasite are present in the kerogen. Analysis of mineral grains shows that Ni is present in both forms of pyrite/marcasite and in the chalcopyrite but not in rutile. The Ni X-ray data also indicates that Ni is present at higher concentrations in the framboidal pyrite than in the massive pyrite. Semiquantitative EMP-XRF data gave Ni concentrations of approximately 0.04 ± 0.02 percent and 0.01 ± 0.01 percent for framboidal and massive type pyrites, respectively. Correction for the Ni content of the kerogen in pyritic form thus cannot be made from the analysis of individual massive pyrite grains.

4. Determination of Inorganic/Organic Associations by the LTA Method.

Previously in this laboratory, the inorganic associations of the elements in kerogens were based upon the LTA of the kerogen (11). In this method the organic matter was oxidized using LTA and the ash was treated with dilute HCl to remove oxides formed in the ashing process. The remaining mineral matter was then considered to be representative of the inorganic fraction of kerogen. In this study a similar procedure was followed for both float and sink kerogen fractions. The ash and HCl-treated ash samples were analyzed by XRD and INAA. The results of these analyses are shown in Table 5. The XRD patterns of both the float and sink ashes revealed the presence of the neoformed fluoride ralstonite. The XRD patterns of the HCl-treated ashes and the trace element data in Table 5 indicate that the ralstonite is soluble in dilute HCl after ashing. Hence, as suggested by Van Berkel and Filby (11) the LTA method cannot be used to determine the organic association of fluorides that precipitate as ralstonite (Na, Mg, Al, etc.) or which coprecipitate with ralstonite.

A major problem with the LTA technique is the partial oxidation of sulfide minerals (pyrite or marcasite) during the ashing procedure. The float ash consistently had a rust color on its surface after a few hours in the asher. This color is a result of the oxidation of pyrite (to Fe_2O_3) as confirmed by the deep yellow color of the HCl wash of the ash and the analytical data in Table 5. Thus, the Fe and other metals leached from oxidized sulfide minerals are not the result of oxidized organic complexes. Because pyrite contains Ni and other transition metal complexes, correction for the contribution of each element in the oxidized pyrite would have to be made. Because the forms of pyrite may have different composition, the correction cannot be based on the composition of the residual pyrite.

CONCLUSIONS

New Albany kerogen concentrates isolated by the scheme shown in Figure 1 were found to contain several residual minerals identified by XRD. Several elements (As, Co, Mo, Mn, Ni, Sb, Se, Zn) appeared to have some association with the major residual mineral, FeS_2, or with other less abundant inorganic forms which were soluble in 3M HNO_3. Of these elements only Mn was found to have no significant contribution to the organic fraction of the kerogen. The remaining elements, along with V, were shown to have substantial organic associations and may be useful in future work on oil-source rock correlations using trace elements.

The results of the two techniques used to quantify the inorganic fraction of the kerogen are compared in Table 6 for the elements mentioned above. The data for the organic compound shows good agreement between the two techniques. For the mineral component agreement for most elements between the two methods is good, except for Mo, Sb, and Se.

It is evident that although the methods allow calculation of organic/inorganic associations of elements in the kerogen isolated from the shale, the "true" concentrations of these elements in the kerogen in the shale cannot be determined. Undoubtably the isolation procedure removes labile elements from the kerogen and adds artifact minerals (ralstonite).

REFERENCES

1. Abu-Elgheit, M., Khalil, S.O., and Barakat, A.O., Prepr. Div. Petrol. Chem. ACS 24, 793-97 (1979).

2. Ellrich, J., Hirner, A., and Stark, H., Chemical Geology 48, 313-23 (1985).

3. Hitchon, B. and Filby, R.H., Bull. Am. Assoc. Petrol. Geol. 68, 838-49 (1984).

4. Curiale, J.A., in "Metal Complexes in Fossil Fuels," R.H. Filby, and J.F. Branthaver, Editors, ACS Symposium Series No. 344, American Chemical Society, Washington, DC, 1987.

5. Van Berkel, G.J., Ph.D. Thesis, Department of Chemistry, Washington State University (1987).

6. Odermatt, J.R., Curiale, J.A., Hirner, H.V., Mercer, G.E. and Filby, R.H., "Determination of Metals in Kerogens: A Comparative Study". Abstract, 197th ACS meeting, Dallas, TX, April 1989.

7. Durand, B. and Nicaise, G., in "Kerogen: Insoluble Organic Matter from Sedimentary Rocks," B. Durand, Editor, Editions Technip, Paris, 1980.

8. Saxby, J.D., in "Oil Shale," T.F. Yen and G.V. Chilingarian, Editors, Elsevier, Amsterdam, 1976.

9. Robinson, W.E., in "Organic Geochemistry", G. Englinton and M.T.J. Murphy, Editors, Springer Verlag, Berlin, 1969.

10. Hasenmueller, N.R., Woodward, G.S. "Studies of the New Albany Shale (Devonian and Mississippian) and equivalent strata in Indiana"; Indiana Geological Survey Contract Report to U.S. Department of Energy, Contract DE-AC-21-76MC05204, 1981; 100 p.

11. Van Berkel, G.J. and Filby, R.H. in "Geochemical Biomarkers", T.F. Yen and J.M. Moldowan, Editors. Horwood Academic Publishers, London, 1988.

12. Van Berkel, G.J., Filby, R.H. and Quirke, J.M.E., Org. Geochem. 14, 119 (1989).

13. Jacobs, F.S., and Filby, R.H. Anal. Chem. 55, 74-7 (1982).

Table 1. Trace element data for New Albany kerogen and density fractions.

Element (μg/g)	Original Kerogen	Float Fraction (d<1.48)	Sink Fraction (d>1.48)	Mineral Residue
Al	4120	3920	11400	2400
As	114	62.7	308	810
Co	130	120	166	187
Cr	41.2	40.1	86	192
Cs	8.16	7.35	21.4	0.838
Fe	48800	17200	177000	376000
Hf	3.09	0.566	10.4	61.0
La	32.6	25.5	79.0	78.8
Mg	2690	<3000	4020	<1500
Mn	47.0	11.5	173	417
Mo	2190	2380	2190	1290
Na	1900	1600	4940	500
Ni	2000	2090	1430	947
Rb	129	135	369	<40
Sb	62.3	70.8	53.7	60.2
Sc	2.90	2.35	7.58	4.56
Se	181	178	202	186
Sm	3.37	3.04	7.01	12.0
Ta	1.93	1.97	2.45	3.33
Ti	2270	730	9540	19000
V	980	1070	541	140
Zn	82.8	78.0	135	258
Zr	154	84.2	442	1960
Mass Used/ Recovered	10.0g	7.9g	1.5g	0.086g

Table 2. Trace element concentrations in mineral and organic components of kerogen calculated from density fractions.

Element (Mg/g)	Concentration in kerogen	Concentration in organic fraction	Concentration in mineral fraction
Al	4120	3117	8991
As	114	36.4	557
Co	130	115	213
Cr	41.2	35.2	133
Cs	8.16	5.84	35.7
Fe	48800	0	340000
Hf	3.09	0	20.4
La	32.6	19.8	133
Mg	2690	--	--
Mn	47.0	0	337
Mo	2190	2400	1997
Na	900	1240	8330
Ni	2000	2160	760
Rb	129	110	606
Sb	62.3	72.6	36.3
Se	2.90	1.79	7.88
Sc	181	175	226
Sm	3.37	2.61	11.0
Ta	1.93	1.92	2.94
Ti	2270	0	18500
V	980	1130	0
Zn	82.8	71.9	193
Zr	154	45.8	805
Float f_{10} = 0.9494		f_{1m} = 0.0506	
Sink f_{20} = 0.4782		f_{2m} = 0.5218	

Table 3. Trace element concentrations in mineral residue sample before and after 3M HNO_3 treatment.

Element (µg/g	Mineral Residue (100%)	HNO_3-Treated Mineral Residue (16%)	Percent Mass Lost
Al	2240	8150	41.8
As	626	38.1	99.0
Co	224	27.1	98.1
Cr	137	829	3.2
Cu	4800	31600	0.0
Cs	1.20	<0.58	--
Fe	390000	32100	98.7
Hf	31.1	182	6.4
La	97.7	12.3	98.0
Mg	1140	1460	79.5
Mn	408	32.1	98.7
Mo	1250	520	93.3
Na	448	814	70.9
Ni	905	1510	73.3
Rb	29.0	<17	--
S	452000	240000	91.5
Sb	40.8	28.3	88.9
Sc	3.37	18.7	11.2
Se	247	649	58.0
Sm	13.8	11.7	86.4
Ta	2.62	16.6	0.0
Ti	8760	66800	0.0
V	98.4	580	5.7
Zn	330	726	64.8
Zr	997	5610	10.0

Table 4. Trace element contents of organic and mineral components for elements showing solubility in dilute HNO_3.

Element (µg/g)	Original Kerogen	Percent Organic	Concentration in Organic Fraction*	Concentration in Inorganic Fraction
As	114	31.1	41.2	540
Co	130	78.5	119	192
Fe	48800	0	0	336000
La	32.6	62.8	23.9	82.5
Mn	47.0	0	0	323
Mo	2190	93.2	2390	1010
Ni	2000	95.8	2240	578
Sb	62.3	71.3	52.0	123
Se	181	90.0	191	124
Zn	82.8	67.2	65.1	187

*Using f_{10} = 0.8546 for kerogen.

Table 5. Trace element data for low temperature ash and HCl-leached ash from kerogen density fractions.

Element (µg/g)	Kerogen* Float 100%	Float Ash 14%	Float Ash-HCl 4.2%	Kerogen Sink 100%	Sink Ash 55%	Sink Ash-HCl 33%
Al	8530	54200	4540	30300	49900	7630
As	64.6	444	340	265	492	564
Co	138	947	590	195	358	228
Cr	31.3	227	240	69.8	125	152
Cs	12.3	88.7	5.87	42.3	74.0	9.19
Fe (%)	1.46	10.5	21.7	13.1	26.2	40.1
Hf	0.299	2.29	7.13	6.53	13.7	19.9
La	36.2	254	33.5	158	274	60.8
Mg	4100	26500	1380	12300	22500	1390
Mn	9.11	61.6	172	166	270	418
Mo	2390	16700	1590	2080	3810	216
Na	2880	20500	1100	10300	18000	2060
Ni	2260	16200	2020	1710	3080	810
Rb	194	1520	197	733	1250	309
Sb	77.7	536	26.9	57.8	102	24.1
Sc	3.69	27.0	2.82	12.6	21.7	5.34
Se	145	576	201	270	396	178
Sm	3.01	22.3	3.85	11.4	20.7	8.46
Ti	<960	<2300	3940	4060	7530	9820
V	911	6480	358	491	950	66.8
Zn	86.1	587	207	145	293	292
Zr	102	602	268	291	542	481

*Percentages refer to mass of original unashed and untreated sample. HCl refers to ash leached with 2M HCl.

Table 6. Comparison of trace element concentrations calculated by the pyrite dissolution method (PDM) to the density fraction method (DFM).

Element (µg/g)	Organic Fraction PDM	Organic Fraction DFM	Inorganic Fraction PDM	Inorganic Fraction DFM
As	41.2	36.4	540	557
Co	119	115	192	213
Fe	0	0	336000	340000
La	23.9	19.8	83.9	133
Mn	0	0	323	337
Mo	2390	2400	1010	2000
Ni	2240	2160	578	760
Sb	52.0	72.6	123	36.3
Se	191	175	124	226
V	1150	1130	0	0
Zn	65.1	11.9	187	193

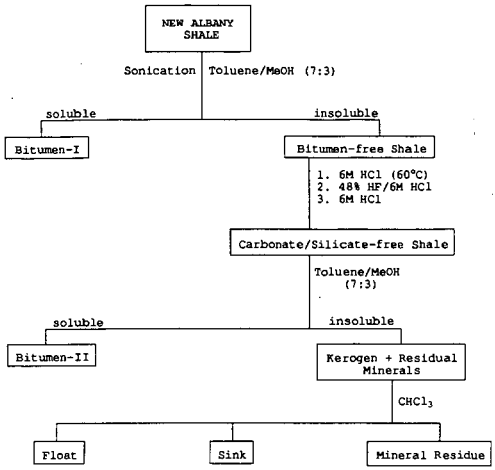

Figure 1: Kerogen Isolation Scheme

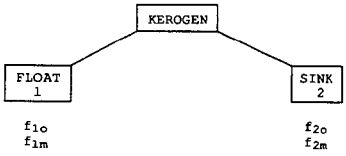

$f_{1o} + f_{1m} = 1$ $\qquad$ $f_{2o} + f_{2m} = 1$

Vanadium concentration organic = V_o
Vanadium concentration mineral = V_m

$V1 = (f_{1o})(V_o) + (f_{1m})(V_m)$ $\qquad$ $V_2 = (f_{2o})(V_o) + (f_{2m})(V_m)$

Assume $V_m << V_o$, Hence

$$\frac{V_1}{V_2} = \frac{f_{1o}}{f_{2o}}$$

For iron, assume $Fe_m >> Fe_o$

$$\frac{Fe_1}{Fe_2} = \frac{f_{1m}}{f_{2m}}$$

Thus, for each element X

$X_1 = (f_{1o})(X_o) + (f_{1m})(X_m)$
$X_2 = (f_{2o})(X_o) + (f_{2m})(X_m)$

f_{1o}, f_{2o} = weight fraction organic in float and sink

f_{1m}, f_{2m} = weight fraction inorganic in float and sink

Figure 2: Calculation of organic/inorganic associations from density fractions

HIGH PRESSURE TPR APPARATUS TO INVESTIGATE ORGANIC SULPHUR FORMS IN COALS.

C.J. Lafferty, C.E. Snape, R. Garcia*, S.R. Moinelo*.
University of Strathclyde
Dept. of Pure and Applied Chemistry
Glasgow G1 1XL
Scotland, United Kingdom.
*Instituto Nacional del Carbon y Sus Derivados
33080 Oviedo
Spain.

ABSTRACT

Temperature programmed reduction (TPR) has been used to investigate the distribution of organic sulphur forms in coals. However, the method used thus far suffers from a number of inherent drawbacks including the low proportion of thiophenic sulphur observed directly and the likelihood of secondary reactions converting sulphides into thiophenes. These drawbacks have largely been overcome using a well swept fixed-bed reactor at relatively high hydrogen pressures (~ 150 bar) with an effective dispersed hydrodesulphurisation catalyst, such as sulphided molybdenum. For three high sulphur coals (a Spanish and a Turkish lignite and a US hvc bituminous coal), levels of desulphurisation were in excess of 90% for the organic sulphur. The first results from the high pressure TPR apparatus with a quadrupole mass spectrometer for on-line analysis of hydrogen sulphide is presented.

1.0 INTRODUCTION

The identification and quantification of the various organic sulphur species in coals is of great importance due to their effects, both beneficial and detrimental, on the subsequent devolatilisation and liquefaction of coal and coal-derived products. At present no established method exists for the direct determination of the distribution of organic sulphur in coal and coal-related products. Several novel techniques have been proposed.

Flash pyrolysis studies on the thermal decomposition of sulphur groups in coal showed that aliphatic sulphur containing groups decompose at much lower temperatures than aromatic groups. However resolution between different aliphatic and aromatic groups was poor[1].

X-ray studies, both surface (XPS)[2,3] and bulk (XANES)[4] characterisation techniques, have shown that it is possible to distinguish between thiophenic and non-thiophenic sulphur groups, however the narrow absorption energy range observed for sulphur containing model compounds coupled with the known number of forms of organic sulphur present in coals results in poor resolution between groups. A larger range is observed for oxidised sulphur

groups[2], it is therefore possible that selective oxidation before x-ray analysis may offer improved resolution.

Another method which has been investigated involves the oxidative pyrolysis of the coal which converts the sulphur into SO_x for subsequent on-line gas analysis, however the resulting resolution between functional groups is generally not as good as that achieved with TPR[5,6] (see following).

In recent years several researchers have been investigating the use of Temperature Programmed Reduction (TPR) for the identification of organic sulphur forms in coal and related products[7,8,9,10]. TPR is based on the principle that each form of organic sulphur exhibits a characteristic reduction temperature, which in a hydrogen rich environment, results in the formation of hydrogen sulphide. The ease of reduction of the various sulphur forms have been found to be in the order thiols > aliphatic sulphides > aromatic sulphides > thiophenes[9]. The current TPR methods generate the hydrogen rich atmosphere by refluxing the coal in a mixture of hydrogen donor solvents[9]. The evolved hydrogen sulphide is swept from the reaction pot by a stream of inert carrier gas at atmospheric pressure. The original method used lead acetate impregnated paper as the H_2S detector[7,9], later workers have used a potentiometric system to measure the evolved H_2S as the sulphide ion, giving a greater degree of quantitation[9]. Sulphur sensitive Flame Photometric Detection (FPD) has also been used however flame stability was found to influence overall sensitivity to a large extent [10].

The TPR method has been the most widely used technique, however at present it contains several limitations which reduce its effectiveness as an analytical technique. The solvent mixture used to generate the hydrogen atmosphere has a relatively low boiling point (< 400°C), consequently complex thiophenes are not detected and must be estimated by difference[10]. Overall sulphur balances are poor, with sulphur of all functionalities remaining in the char after analysis, possibly due to mass transfer limitations inherent to the reaction pot, which could result in retrogressive reactions including transformation of aliphatic sulphides to thiophenes[11,12]. Finally, the overall contribution of pyrite to the evolved H_2S signal, particularly the transformation of pyrite to pyrrhotite and to iron with the subsequent evolution of H_2S appears to have been overlooked or considered negligible by previous researchers.

This paper presents results obtained for three high sulphur coals from a high pressure fixed bed hydropyrolysis reactor which is relatively unaffected by any mass transfer effects and any associated retrogressive reactions resulting in effective desulphurisation, including the removal of complex thiophenes. This reactor has been modified through the fitting of a suitable gas analysis system to form a TPR reactor.

2.0 EXPERIMENTAL

Table 1 lists the ultimate analyses and sulphur distributions of the coal samples studied.

The hydropyrolysis reactor has been described previously[13]. The desulphurisation experiments were conducted on a 5g scale at 520°C using a gas velocity of ~ 0.2 m s^{-1} to virtually overcome mass transfer limitations to volatile release. For each coal (75-200um), three tests were conducted using a pressure of (i) 150 bar nitrogen and (ii) 150 bar hydrogen with and without a sulphided molybdenum (Mo) catalyst (1% loading prepared from ammonium dioxydithiomolybdate[13]). In addition, the thermal desulphurisation of the three coals was also investigated in the temperature range 250-500°C using the BS volatile matter test (BS1016).

For the TPR runs, a smaller but otherwise identical reactor system was used. 2g of coal was heated from ambient to 570°C at 2°Cmin^{-1}. The hydrogen pressure was again 150 bar and the gas velocity ~ 0.2 m s^{-1}. On line analysis of the gas stream for H_2S and other gaseous products is performed using a quadrupole mass spectrometer in multiple ion monitoring mode. The atmospheric pressure side of the exit stream from the reactor was connected to the mass spectrometer by a 1.8 m length of heated capillary tubing sampling at a rate of 25 ml min^{-1}. The reactor thermocouple signal is also fed to the mass spectrometer allowing direct plots of evolved gas concentration against bed temperature to be generated.

Concentrations of pyritic and pyrrhotitic sulphur in the chars were determined. FTIR was used to compare the relative amounts of sulphatic sulphur in the chars and corresponding low temperature ash samples, sulphate absorbances occurring in the range 1110-1150 cm^{-1}. Gas chromatography (GC) with mass spectrometric (MS) and flame photometric detection (FPD) were carried out to compare the distribution of thiophenic compounds in the tars.

3.0 RESULTS AND DISCUSSION

3.1 DESULPHURISATION

Table 1 lists the distribution of sulphur forms in the original coals and Table 2 summarises the char and tar yields for the desulphurisation tests as well as the sulphur distributions in the pyrolysis products. The two lignites gave broadly comparable tar yields and total conversions in corresponding tests, but these were slightly higher than those obtained for Bevier-Wheeler coal. As anticipated, the total conversions increased in going from pyrolysis to high pressure hydropyrolysis and catalytic hydropyrolysis (Table 2). The extent of desulphurisation (sulphur in gas plus tar as a percentage of that in the original coal) increased with increasing conversion (Table 2) but a number of marked differences were found for the coals investigated.

In Table 2 it has been assumed that sulphatic sulphur remains in the chars and is unaffected by pyrolysis. Indeed, only small differences were found in the absorbances of the characteristic IR sulphatic bands at 1110-1150 cm^{-1} between the chars and the corresponding low temperature ashes when the spectra were normalised to 1mg cm^{-2} of mineral matter. For all three coals, significantly more pyrite is reduced during high pressure hydropyrolysis than in pyrolysis (Table 2). The ease of pyrite reduction to pyrrhotite and iron is greatest for Bevier-Wheeler coal and optical microscopy has shown that it would appear to correlate with the size of pyrite particles in the coal. For the lignites, much of the pyrite occurs as fine grains dispersed in both the organic and mineral matter. In Bevier-Wheeler coal, the pyrite is mainly present as relatively large particles which are presumed to be more accessible to hydrogen than fine grains.

The three coals display completely different trends for the removal of organic sulphur (Table 2). For Cayirhan lignite, nearly all of the organic sulphur is eliminated as tar and gas in pyrolysis compared with ~75% for Mequinenza lignite.The implication is clearly that little of the organic sulphur exists in condensed thiophenic structures for Cayirhan lignite. Indeed, nearly all the organic sulphur is also removed in the standard volatile matter test at 500°C with ~ 20% being eliminated below 250°C (Figure 1). The fact that much more of the sulphur is released from the Cayirhan lignite below 250°C (Figure 1) implies that this lignite contains a greater proportion of aliphatic sulphides/thiols than Mequinenza lignite. However there is the strong possibility that some thiophenic sulphur results from cyclisation and aromatisation of non-thiophenic forms during pyrolysis[11,12]. As anticipated, the extent of organic sulphur removal is low for Bevier-Wheeler coal with only ~ 20% being eliminated in pyrolysis and also at 500°C in the volatile matter test (Table 2 and Figure 1). However, in catalytic hydropyrolysis the proportion eliminated is ~ 90%.

For Mequinenza lignite, GC has shown that thiophenes are the dominant species over benzo- and dibenzothiophenes in the pyrolysis tar. However, in the high pressure hydropyrolysis tars, thiophenes are present in trace amounts which is consistent with the greater ease of hydrodesulphurisation of single ring thiophenes. For Cayirhan lignite, benzothiophenes are the major thiophene class present in the pyrolysis tar but in going to catalytic hydropyrolysis, dibenzothiophenes and other high molecular weight thiophenes become the dominant species.

3.2 HIGH PRESSURE TEMPERATURE PROGRAMMED REDUCTION

Figure 2 shows the H_2S evolution trace for Mequinenza lignite (A) untreated and (B) impregnated with the molybdenum catalyst. The higher resolution trace obtained without catalyst shows seven distinct peaks which can be assigned to various functional groups based on characteristic reduction temperatures identified in earlier studies [9]. At present, studies are under way to confirm

the reduction temperatures of various model compounds in the swept bed TPR reactor.

The trace for the catalyst impregnated sample shows a loss of fine resolution, but more thiophenic sulphur is detected around 300-400°C, and over a smaller temperature range than for the untreated sample. The loss of resolution may be as a result of a continual adsorption/desorption of H_2S on the hot catalyst surface. Different catalyst compositions and loadings will be investigated in order to improve the resolution observed for catalyst impregnated coals.

4.0 CONCLUSIONS

The use of a fixed bed pyrolysis reactor swept with high velocity hydrogen has been shown to effectively desulphurise high sulphur coals. The reactor is relatively unaffected by any mass transport limitations and as a result, retrogressive sulphur transformations are avoided. The reactor system has been adapted to enable the characterisation of organic sulphur species within the coals via high pressure temperature programmed reduction and initial results have shown a high degree of resolution between functional groups.

5.0 ACKNOWLEDGEMENTS

The authors acknowledge funding provided by the Science and Engineering Research Council (Project No. GR/G/26600) and by DGICYT (Project No.PB87-0417).

6.0 REFERENCES

1. Calkins W.H., 1985, Am. Chem. Soc. Div. Fuel Chem., prepr., 30(4), 450.
2. Jones R.B., McCourt C.B. and Swift P., Proc. 1981 Int. Conf. on Coal Science (IEA). 657.
3. Keleman S.R., George G.N. and Gorbaty M.L., 1990, Fuel, 69, 939.
4. Gorbaty M.L., George G.N. and Keleman S.R., 1990, Fuel, 69, 945.
5. Boudou J.P., Boulegue J., Malechaux L., Nip M., de Leeuw J.W. and Boon J.J., 1987, Fuel, 66, 1558.
6. La Count R.B., Anderson R.R., Friedman S. and Blaustein B.D., 1987, Fuel, 66, 909.
7. Attar A., 1983, DOE/PC/30145TI Technical Report.
8 Attar A., in C. Karr (Ed), Analytical Methods for Coal and Coal Products, Vol III, Academic Press, 1979. Ch. 56.
9. Majchrowicz B.B., Franco D.V., Yperman J., Reggers G., Gelan J., Martens H., Mullens J. and van Poucke L.C., 1991, Fuel, 70, 434.
10. Dunstan B.T. and Walker L.V., 1988, Final Report to Australian National Energy Research Development and Demonstration Council.
11. Keleman S.R., George G.N., Gorbaty M.L., Kwiatek, P.J. and Sansone, M., 1991, Fuel, 70, 396.

12. Cleyle P.T., Caby W.F., Stewart, I. and Whiteway S.G., 1984, Fuel, 63, 1579.
13. Snape C.E. and Lafferty C.J., 1990, Am. Chem. Soc. Div. Fuel Chem., prepr., 35(1), 1.

Table 1. Ultimate and Sulphur Analyses of Coal Samples

		Lignites		hvc Bituminous PSOC 1409
		Mequinenza (Spain)	Cayirhan (Turkey)	Bevier-Wheeler (Nth America)
(% daf)	C	66.4	64.3	76.9
	H	5.8	5.1	5.5
	N	1.6	2.3	1.8
Sulphur (% db)	Total	9.0	4.8	6.8
	Pyritic	0.5	1.0	4.0
	Sulphate	0.5	0.9	0.3
	Organic	8.0	2.9	2.5

Table 2. Distribution of Sulphur in Pyrolysis Products (% Original Sulphur in Coal)

	% Yield		Char					Tar	Gas*	%DS
	Char	Tar	S_T	S_p	$S^=$	S_{SO4}	S_o*			
Mequinenza			100	6	<1	6	88			
Py	53	33	38	4	1	6	27	25	37	62
Hypy	27	50	13	1	2	6	4	18	69	87
C.Hypy	13	63	10	1	2	6	1	23	67	90
Cayirhan			100	21	<2	19	54			
Py	49	39	45	16	5	19	<1	20	35	55
Hypy	25	57	27	1	6	19	<1	11	62	73
C.Hypy	16	63	22	1	1	19	<1	12	66	78
Bevier Wheeler			100	59	<1	5	36			
Py	63	25	61	10	16	5	30	7	32	39
Hypy	39	48	27	2	9	5	11	9	64	73
C.Hypy	30	56	20	1	11	5	3	6	74	80

* := by difference
S_T := Total sulphur
S_p := Pyritic sulphur
%DS := % Desulphurisation
$S^=$:= Pyrrhotitic sulphur
S_{SO4} := Sulphatic sulphur
S_o := Organic sulphur

SULPHUR REMOVAL IN VOLATILE MATTER TESTS

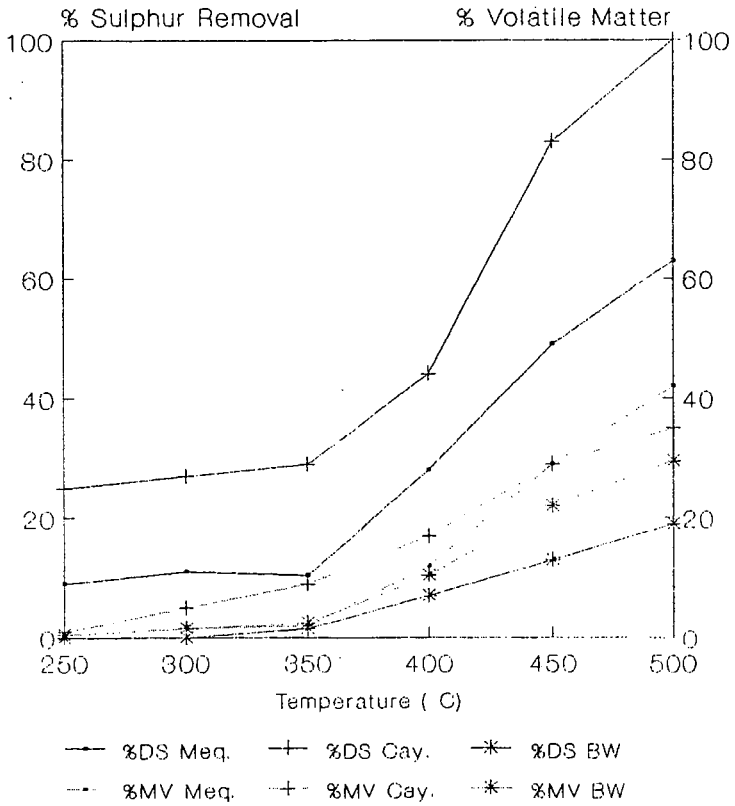

Fig.1. Desulphurisation and Volatile Matter Yields.

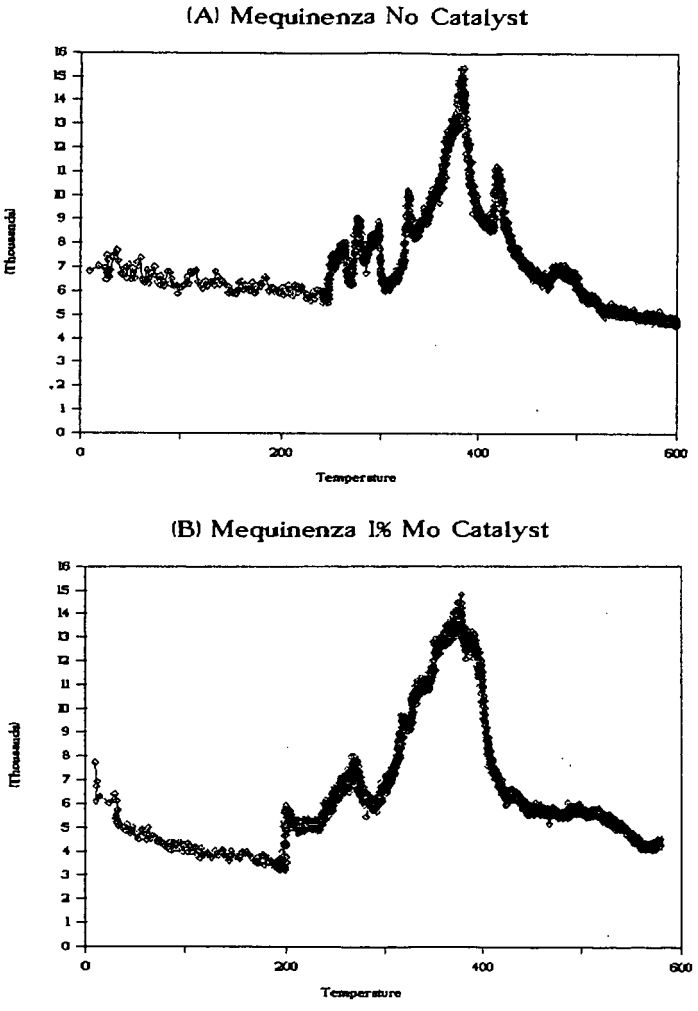

Fig. 2. TPR Traces for Mequinenza Lignite